Multiviral Quartet Nanocages Elicit Broad Anti-Coronavirus Responses for Proactive Vaccinology

Rory A. Hills[1,2], Tiong Kit Tan[3], Alexander A. Cohen[4], Jennifer R. Keeffe[4], Anthony H. Keeble[1,2], Priyanthi N.P. Gnanapragasam[4], Kaya N. Storm[4], Michelle L. Hill[5], Sai Liu[5], Javier Gilbert-Jaramillo[5], Madeeha Afzal[5], Amy Napier[5], William S. James[5], Pamela J. Bjorkman[4], Alain R. Townsend[3,6]* and Mark Howarth[1,2]*

[1]Department of Biochemistry, University of Oxford, South Parks Road, Oxford, OX1 3QU, UK.
[2]Department of Pharmacology, University of Cambridge, Tennis Court Road, Cambridge, CB2 1PD, UK.
[3]MRC Human Immunology Unit, MRC Weatherall Institute of Molecular Medicine, John Radcliffe Hospital, University of Oxford, Oxford, OX3 9DS, UK.
[4]Division of Biology and Biological Engineering, California Institute of Technology, Pasadena, CA 91125, USA.
[5]James & Lillian Martin Centre, Sir William Dunn School of Pathology, University of Oxford, South Parks Road, Oxford, OX1 3RE, UK.
[6]Centre for Translational Immunology, Chinese Academy of Medical Sciences Oxford Institute, University of Oxford, Oxford, OX3 7BN, UK.

*Corresponding authors and Lead Contacts:
Mark Howarth,
Department of Pharmacology,
University of Cambridge,
Tennis Court Road,
Cambridge,
CB2 1PD,
UK
E-mail: mh2186@cam.ac.uk
and
Alain R. Townsend,
MRC Human Immunology Unit,
MRC Weatherall Institute of Molecular Medicine,
John Radcliffe Hospital,
University of Oxford,
Oxford,
OX3 9DS,
UK.
E-mail: alain.townsend@imm.ox.ac.uk

Abstract
Defending against future pandemics may require vaccine platforms that protect across a range of related pathogens. The presentation of multiple receptor-binding domains (RBDs) from evolutionarily-related viruses on a nanoparticle scaffold elicits a strong antibody response to conserved regions. Here we produce quartets of tandemly-linked RBDs from SARS-like betacoronaviruses coupled to the mi3 nanocage through a SpyTag/SpyCatcher spontaneous reaction. These Quartet Nanocages induce a high level of neutralizing antibodies against several different coronaviruses, including against viruses not represented on the vaccine. In animals primed with SARS-CoV-2 Spike, boost immunizations with Quartet Nanocages increased the strength and breadth of an otherwise narrow immune response. Quartet Nanocages are a strategy with potential to confer heterotypic protection against emergent zoonotic coronavirus pathogens and facilitate proactive pandemic protection.

Keywords:
outbreak pathogens; bioconjugation; nanobiotechnology; synthetic biology; Covid-19; zoonotic

One Sentence Summary
A vaccine candidate with polyprotein antigens displayed on nanocages induces neutralizing antibodies to multiple SARS-like coronaviruses.

Main
SARS-CoV-2 (SARS2) has caused at least 6 million deaths and new variants continue to emerge (*1*). Despite the success of vaccination in reducing death and serious illness, waning vaccine protection and uncertain efficacy of therapeutics mean that new vaccine strategies are still urgently needed (*2*, *3*). It is also important to protect against new pandemic threats from coronaviruses, which previously led to SARS-CoV (SARS1) and MERS-CoV outbreaks (*4*) and which includes other bat viruses with pandemic potential such as WIV1 and SHC014 (*5*). Immunizing with a single antigen typically induces a narrow strain-specific immune response that may not protect against diverse pre-existing strains or newly arising variants of that pathogen (*6*).

Antigen resurfacing and masking of non-protective regions with glycosylation have been attempted to focus antibody responses on regions of low variability and produce more broadly effective vaccines. However, these strategies can lead to overly specific immune responses susceptible to pathogen escape and have not reliably increased neutralization efficacy (*7*, *8*). Both strategies have been employed on the Receptor-Binding Domain (RBD) of SARS2 Spike. RBD is directly involved in binding to the cell receptor angiotensin-converting enzyme 2 (ACE2) and is the target of most neutralizing antibodies (*9*). Many vaccines have employed RBD as the immunogen and fusion of two SARS2 RBDs into a tandem homodimer was employed early in the COVID-19 pandemic to enhance the immune response, leading to a licensed vaccine (*10*). A tandem heterotrimer composed of one RBD from Wuhan, Beta and Kappa SARS2 has entered clinical development (*11*). Another strategy involves fusion of individual RBDs to proliferating cell nuclear antigen (PCNA) to make a ring with 6 protruding antigens (*12*). However, low molecular weight immunogens may be insufficient to give strong and long-lasting protection (*13*). Highly multivalent display on larger virus-like particles (VLPs) or other nanoparticles enhances the strength and persistence of immune responses, facilitating lymph node uptake and increasing B cell receptor clustering (*13*, *14*). VLP manufacturing uses existing facilities for microbial fermentation to facilitate

production of billions of doses (*15*), can avoid the need for a cold-chain (*16*), and has shown a good balance of safety and efficacy (*17*).

In a recently introduced approach, VLPs display a panel of protein variants to favor expansion of B cells recognizing common features of the different antigens. For example, a mosaic of different hemagglutinin heads on ferritin nanoparticles elicited cross-reactive antibodies against diverse influenza strains within the H1 subtype (*18*). This approach has been applied to SARS2, based upon mosaic nanoparticles displaying multiple RBDs from different sarbecoviruses (*6*, *19*, *20*). Sarbecoviruses are the sub-genus of betacoronaviruses that includes SARS1 and SARS2. RBDs can be attached to a VLP through genetic fusion (*20*) or isopeptide coupling (*6*). We previously demonstrated that fusion of a set of sarbecovirus RBDs with SpyTag003 facilitated simple assembly onto the SpyCatcher003-mi3 VLP (*6*) (Fig. 1A). SpyCatcher003 is a protein engineered to rapidly form an isopeptide bond with SpyTag peptide (*21*). mi3 is a 60-mer hollow protein nanocage, computationally designed to self-assemble into a stable dodecahedron (*22*, *23*). In our previous study, the broadest immune response came from mosaic particles displaying 8 different RBDs in a stochastic arrangement (*6*, *19*). These Mosaic-8 nanoparticles elicited neutralizing antibodies against a variety of sarbecoviruses in mouse and rhesus macaque models. Critically, responses were not limited to viruses whose RBDs were represented on Mosaic-8 nanoparticles and included mismatched responses against heterologous sarbecoviruses (*6*, *19*). Mosaic-8 nanoparticles have gained support from the Coalition for Epidemic Preparedness Innovations (CEPI) to enter clinical trials. However, there may be challenges in broad scaling because of the need to produce 9 different components (8 RBDs and SpyCatcher003-mi3) at Good Manufacturing Practice (GMP) level.

Here we establish the production of a multiviral Quartet Nanocage (Fig. 1A). Initially we express a multiviral Quartet from RBDs of 4 different viruses linked as a single polypeptide chain. These antigenic Quartets are assembled via a terminal SpyTag onto SpyCatcher003-mi3 nanocages, creating a protein nanoparticle with dendritic architecture. In addition to reducing the number of vaccine components, this strategy allows a greater number of RBDs to be displayed on each nanocage. We measure antibody responses to the range of sarbecoviruses displayed on the Quartet Nanocage, to sarbecoviruses not present within the chain, as well as to SARS-CoV-2 variants of concern (VOCs). We dissect the breadth of binding to different sarbecoviruses, neutralization potency, and the ability to boost a broad response following focused priming. The magnitude and breadth of antibody induction show that Quartet Nanocages may provide a scalable route to induce neutralizing antibodies across a range of related viruses, to prepare for emerging outbreak disease threats.

Design of multiviral Quartet Nanocages

RBDs from the evolutionarily-related sarbecoviruses SHC014, Rs4081, RaTG13 and SARS2 Wuhan (Fig. 1B) were genetically fused to produce a multiviral Quartet (Fig. 1C). These RBDs allow comparison to the previously described Mosaic-4 vaccine (*6*). SHC014 can mediate infection of human cells and has been identified as a zoonotic spill-over risk (*24*). Rs4081 is capable of infecting human cells (*25*) but does not enter via ACE2 (*26*). RaTG13 was identified in the intermediate horseshoe bat (*Rhinolophus affinis*) and shares 90% sequence identity for its RBD with SARS2 (Fig. S1 and S2) (*27*). The multiviral Quartet was engineered with a signal sequence for secretion from mammalian cells and a terminal SpyTag, to enable multivalent display on SpyCatcher003-mi3 nanocages (Fig. 1A). The Quartet was secreted efficiently by Expi293F cells and affinity-purified via SpyTag using the SpySwitch system (*28*) (Fig. S3). The Quartet band was relatively broad on SDS-PAGE because of natural variation in glycosylation (Fig. 1D). Removal of N-linked glycans with Peptide N-Glycosidase F

(PNGase F) induced a downward shift in protein mobility and a uniform band (Fig. 1D). We demonstrated that the Quartet coupled efficiently to SpyCatcher003-mi3 (Fig. 1E).

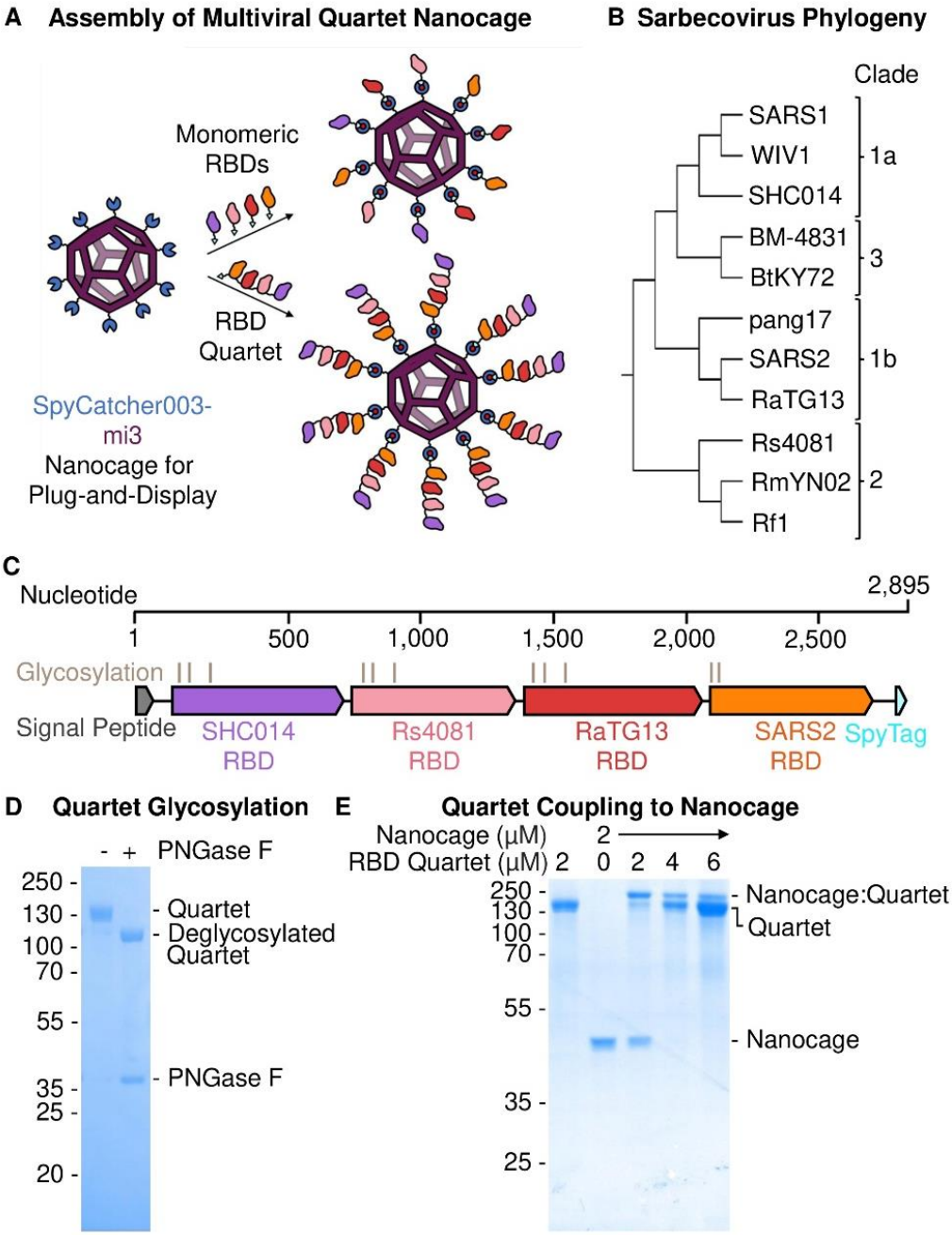

Fig. 1 Preparation of Multiviral Quartet. (**A**) Plug-and-Display vaccine assembly of mosaic and Quartet Nanocages. Genetic fusion of SpyCatcher003 (dark blue) with mi3 (purple) allows efficient multimerization of single or Quartet RBDs linked to SpyTag (cyan) through spontaneous isopeptide bond formation (marked in red). Only some antigens are shown in the schematic for clarity. (**B**) Phylogenetic tree of sarbecoviruses used in this study, based on RBD sequence. (**C**) Genetic organization of the multiviral Quartet-SpyTag, indicating the viral origin of RBDs, N-linked glycosylation sites, and tag location. (**D**) Analysis of Quartet-SpyTag with SDS-PAGE/Coomassie staining, with or without PNGase F deglycosylation. (**E**) Coupling of RBD Quartet to SpyCatcher003-mi3 nanocage at different molar nanocage:antigen ratios, analyzed by SDS-PAGE/Coomassie.

Quartet Nanocages induce antibody responses to diverse sarbecoviruses

We then explored the Quartet's immunogenicity as a soluble protein or displayed on nanocages, in comparison to a monomeric SARS2 RBD (Fig. 2A). Doses for all immunizations were normalized by the number of SpyTags, allowing comparison of a molar equivalent of SpyCatcher003-mi3 nanocages with similar levels of occupancy. For Uncoupled RBD, this dose of 0.02 nmol corresponds to 0.6 µg protein. Two doses were administered to mice 14 days apart using alum-based adjuvant (Fig. 2B), before quantifying IgG titer against RBD antigens by ELISA. Post-prime, the Quartet Nanocage elicited the highest antibody titer against SARS2 Wuhan RBD, surpassing the Homotypic Nanocage and Uncoupled Quartet (Fig. S4A). Unless indicated, SARS2 responses are measured with Wuhan RBD. We also assessed antibody response to SARS1 RBD, not represented in the immunogens, reflecting induction of broader anti-sarbecovirus antibodies. Here Homotypic Nanocage elicited a weak response against SARS1 but there was still a substantial response from Quartet Nanocage (Fig. S4A). The titer against SARS1 from Quartet Nanocage was greater than the response against SARS2 by Homotypic Nanocage (Fig. S4A).

After boosting, again we found the strongest response against SARS2 from Quartet Nanocage, followed by Uncoupled Quartet, Homotypic Nanocage, and finally Uncoupled RBD (Fig. 2C). This pattern is retained for SARS2 Wuhan, Beta, and Delta Spike (Fig. S4B). After immunizing with Uncoupled RBD or Homotypic Nanocage, responses were very low against other sarbecovirus RBDs (SHC014, Rs4081, RaTG13, SARS1 and BM-4831) (Fig. 2C). However, we saw substantial response against other sarbecovirus RBDs with Uncoupled Quartet and the highest response with Quartet Nanocage (Fig. 2C). We had hypothesized that RBDs exposed at the tip of the Quartet would give stronger responses than RBDs nearer the nanocage surface. In fact, we saw no obvious relationship between the RBD chain location and antibody titer (Fig. 2C). In addition, Quartet Nanocage raised a strong heterotypic response against BM-4831 and SARS1 RBDs absent from the chain, with titers only slightly lower than Homotypic Nanocage against SARS2 (Fig. 2C). Homotypic Nanocage induced its highest cross-reactive response against the closely related RaTG13 RBD, with minimal titers against all other RBDs (Fig. 2C). These results suggest the potential of this Quartet Nanocage approach to induce antibody responses against a broad range of sarbecoviruses.

Comparison of antibody responses induced by Quartet Nanocages and Mosaic nanoparticles

We next compared the multiviral Quartet to leading mosaic nanoparticle vaccines. Mosaic-4, containing the same 4 RBDs as our Quartet, had induced broad antibodies, but the best breadth was obtained with a Mosaic-8 immunogen (*6, 19*). Therefore, we also produced the Alternate Multiviral Quartet, containing SpyTag followed by RBDs from other sarbecoviruses: pang17, RmYN02, Rf1 and WIV1 (Fig. S5B). Coupling both the Quartet and Alternate Quartet to SpyCatcher003-mi3 generated the Dual Quartet Nanocage, presenting the same 8 RBDs as Mosaic-8 (Fig. 3A). The Alternate Quartet was efficiently expressed by Expi293F cells and we similarly characterized the protein by SDS-PAGE/Coomassie with and without deglycosylation using PNGase F (Fig. 3B). To interrogate further the relationship between chain position and immunogenicity, we produced a Quartet with SpyTag moved from the C-terminus to the N-terminus (Fig. S5A). This SpyTag-Quartet was used for all subsequent immunizations.

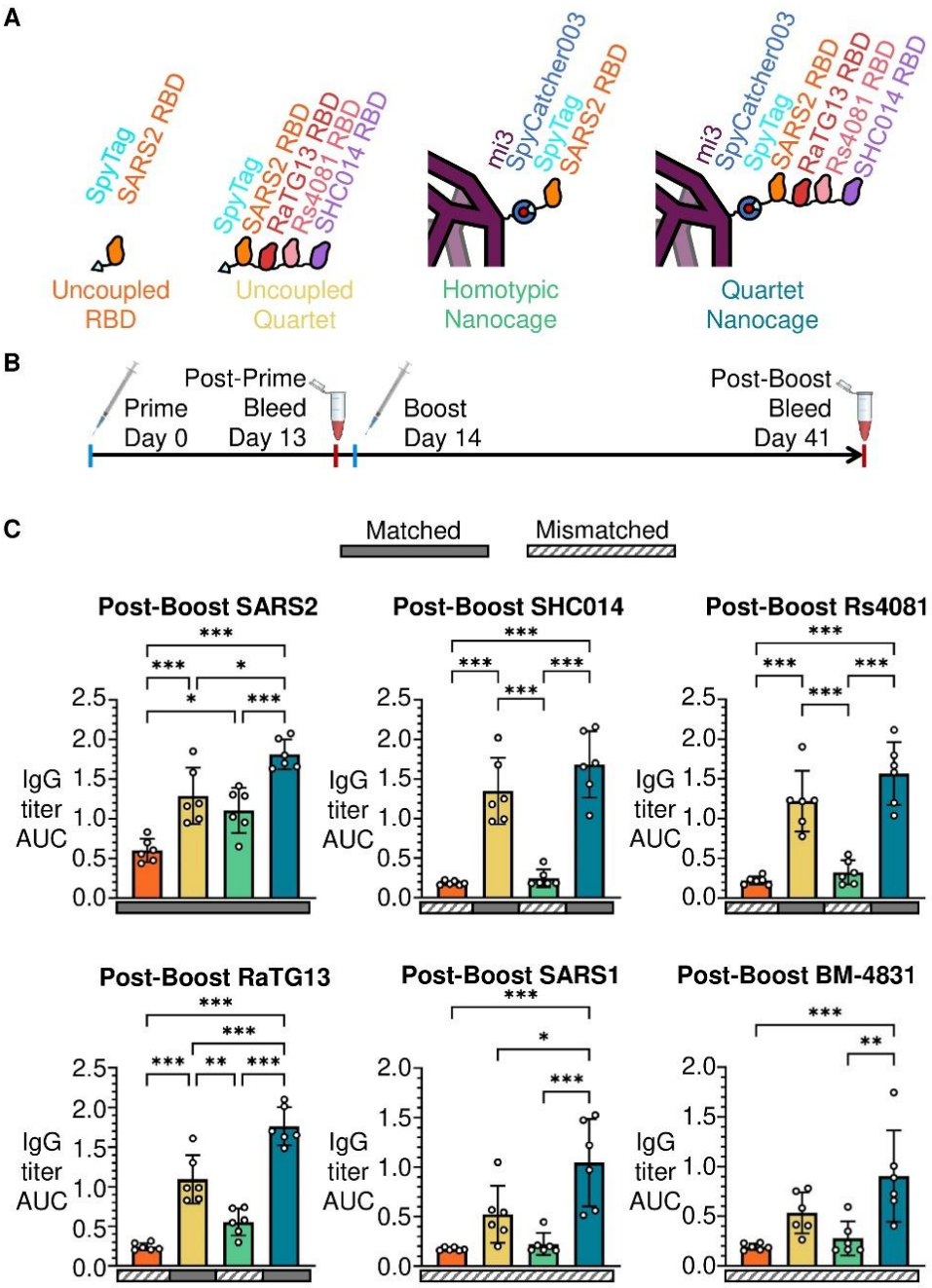

Fig. 2 Broad Immune Response from Immunization with Quartet Nanocages. (**A**) Schematic of antigens for this set of immunizations, comparing uncoupled proteins or proteins coupled to the SpyCatcher003-mi3 nanocage. (**B**) Procedure for immunization and sampling. (**C**) ELISA for post-boost serum IgG binding to different sarbecovirus RBDs is shown as the area under the curve (AUC) of a serial dilution. Sera are from mice immunized with uncoupled SARS2 RBD (orange), uncoupled Quartet-SpyTag (yellow), SARS2 RBD coupled to SpyCatcher003-mi3 (green), or Quartet-SpyTag coupled to SpyCatcher003-mi3 (blue). Solid rectangles under samples indicate ELISA against a component of that vaccine (matched). Striped rectangles indicate ELISA against an antigen absent in that vaccine (mismatched). Each dot represents one animal. The mean is denoted by a bar, shown ± 1 s.d., n = 6. * $p < 0.05$, ** $p < 0.01$, *** $p < 0.001$; other comparisons were non-significant.

To compare Mosaic and Quartet Nanocage immunogenicity, we employed a prime-boost approach and analyzed antibody titers, comparing Mosaic-4 and Mosaic-8 with the Quartet Nanocage, Dual Quartet Nanocage, and Uncoupled Quartet (Fig. 3A). Dynamic Light Scattering (DLS) validated that each immunogen homogeneously assembled with SpyCatcher003-mi3 (Fig. 3C). For all RBDs, the two highest post-boost antibody titers were raised by Quartet Nanocage and Dual Quartet Nanocage (Fig. 3D, Fig. S6, Fig. S7). Surprisingly, Quartet Nanocage and Dual Quartet Nanocage induced a similar response to each other against WIV1 and pang17 (Fig. 3D, Fig. S7), even though these antigens were present in Dual Quartet Nanocage but not Quartet Nanocage. In agreement with previous results (*6*), Mosaic-4 and Mosaic-8 produced higher titers than SARS2 Homotypic Nanocage against the RBD set, which were statistically significant with the exception of SARS2. Uncoupled Quartet produced similar titers as both Mosaics against the RBD set, with no statistically significant difference (Fig. 3D, Fig. S6, Fig. S7). These trends were also apparent in post-prime samples, except Mosaic-8 and Quartet Nanocage raised a similar anti-SARS1 response (Fig. S6B). As previously, there was no clear relationship between chain position and antibody response against that RBD. All conditions except Uncoupled Quartet induced a comparable antibody response against SpyCatcher003-mi3 itself (Fig. S6C). SpyTag-Maltose Binding Protein (MBP) was used as a negative control, which revealed minimal antibody response against SpyTag itself (Fig. S6C).

To relate antibody level to antibody efficacy, we tested neutralization of SARS2 Wuhan or Delta virus. We saw the strongest neutralization induced by Quartet Nanocage in each case, while Homotypic Nanocage gave higher responses than Uncoupled Quartet (Fig. 4A, Fig. 4B). To analyze the breadth of neutralizing antibodies, we investigated SARS1 pseudovirus, setting a difficult challenge because SARS1 is a mismatch for all immunogens. Pseudotyped virus neutralization assays correlate well with neutralization of authentic virus (*29*). For this system, we also compared Quartet Nanocage to Mosaic-4 and Mosaic-8. Out of all the immunogens, Dual Quartet Nanocage gave the strongest neutralizing response to SARS1. This was followed by Quartet Nanocage and Mosaic-8, which induced relatively strong and equivalent response against SARS1, while Mosaic-4, Homotypic Nanocage and Uncoupled Quartet gave lower neutralizing responses (Fig. 4C).

We gained additional insight using 10-fold higher antigen dose and the squalene-based adjuvant AddaVax to enhance viral neutralization further (Fig. S8A). For post-boost sera, there was no significant difference between the antibody titer to SARS2 RBD for any tested vaccine candidate (Fig. S8B). However, the Homotypic Nanocage antibody titer to SARS1 and BtKY72 RBDs were significantly lower than those raised by any of the other conditions, except for the Quartet Nanocage response to SARS1 where the difference did not reach significance (Fig. S8B). Unlike lower-dose immunizations, there was no significant difference between the antibody titer raised by the Mosaic-8, Quartet Nanocage, or Dual Quartet Nanocage to the mismatched SARS1 and BtKY72 RBDs (Fig. S8B). Mosaic-8, Quartet Nanocage, and Dual Quartet Nanocage all elicited favorable neutralization of WIV1, SARS1, and SHC014 pseudovirus (Fig. S8C, Fig. S9). Neutralization of BtKY72 pseudovirus was strong for Mosaic-8 and Dual Quartet Nanocage but less effective for Quartet Nanocage (Fig. S8C). In all cases, Homotypic Nanocage elicited the weakest neutralization of these pseudoviruses (Fig. S8C, Fig. S9A). Under high-dose conditions there was no clear pattern between neutralization by the different immunogens to SARS2 Wuhan, Beta, Delta, and Omicron BA.1 (Fig. S9B, Fig. S10). No immunogen elicited substantial neutralization of SARS2 Omicron XBB.1 pseudovirus (Fig. S9A) or authentic Omicron BQ.1.1 virus using this immunization schedule (Fig. S10), which is consistent with the exceptional immune evasion found for Omicron variants (*30*).

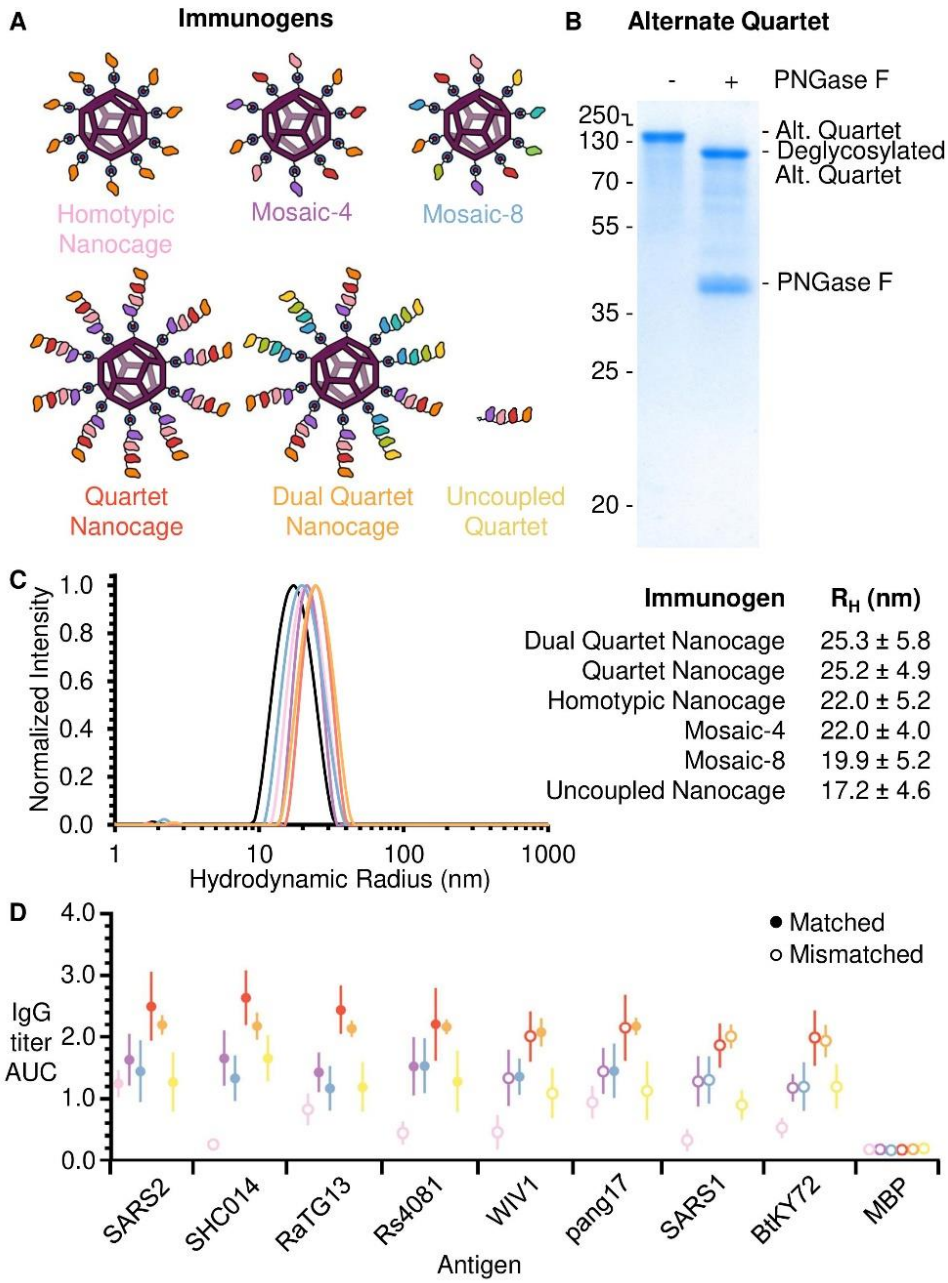

Fig. 3 Comparison of immunization with Mosaic or Quartet Nanocages. (**A**) Schematic of antigens for this set of immunizations. (**B**) Validation of the Alternate Quartet by SDS-PAGE with Coomassie staining, shown ± PNGase F deglycosylation. (**C**) DLS of SpyCatcher003-mi3 alone (uncoupled nanocage) or each immunogen. The mean hydrodynamic radius (R_H) is shown ± 1 s.d., derived from 20 scans of the sample. Uncoupled Nanocage is shown in black, with the other particles colored as in (A). **(D**) ELISA for post-boost serum IgG as the area under the curve of serial dilution, from mice immunized with Homotypic SARS2 Nanocages (pink), Mosaic-4 (purple), Mosaic-8 (blue), SpyTag-Quartet Nanocage (red), Dual Quartet Nanocage (orange), or Uncoupled Quartet (yellow). Filled circles indicate ELISA against a component of that vaccine (matched) while empty circles indicate ELISA against an antigen absent in that vaccine (mismatched). Responses are shown to the set of sarbecovirus RBDs, with SpyTag-MBP as a negative control. The mean is denoted by a circle, shown ± 1 s.d., n = 6. Individual data points and statistics are shown in Fig. S6 and S7.

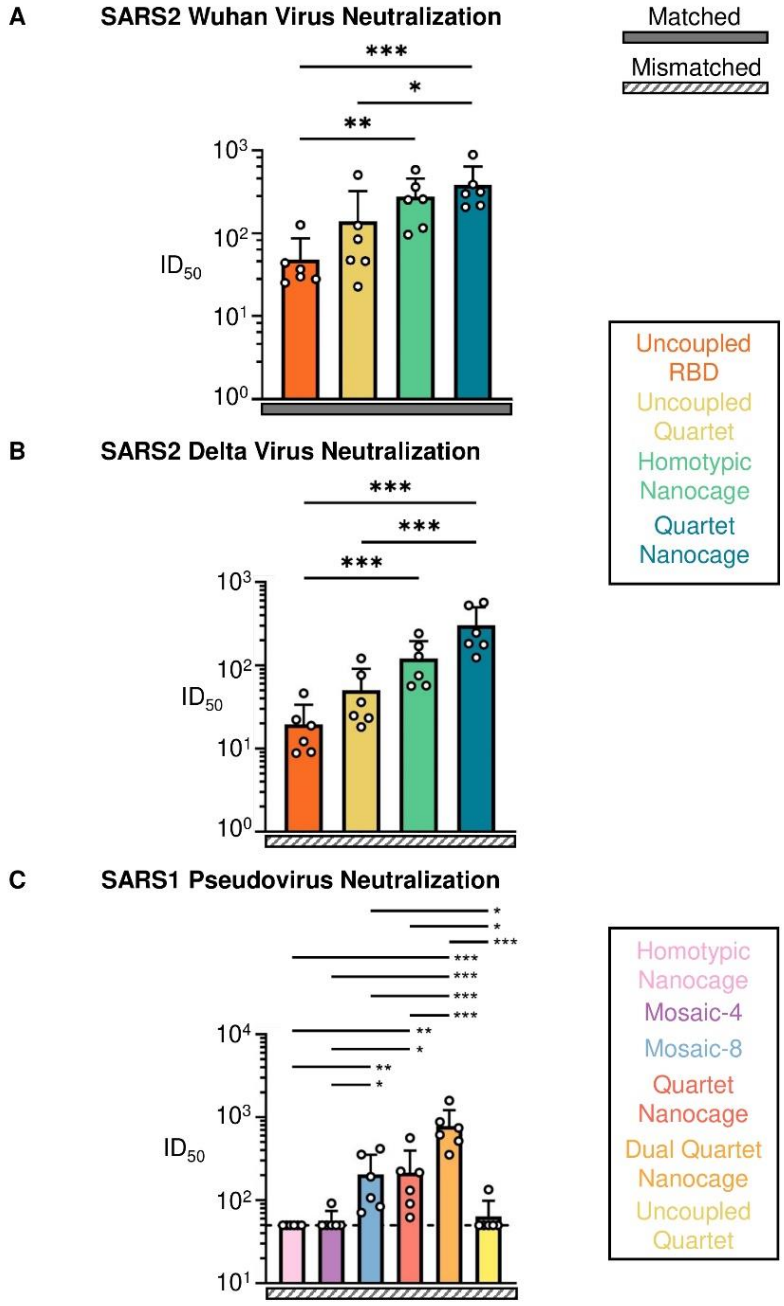

Fig. 4 Neutralization induced by Quartet immunogens. (**A**) Neutralization of Wuhan SARS2 virus by boosted mouse sera. Mice were primed and boosted with Uncoupled RBD (orange), Uncoupled Quartet (yellow), Homotypic Nanocage (green), or Quartet Nanocage (blue). Each dot represents one animal, showing the serum dilution giving 50% inhibition of infection (ID_{50}). (**B**) Neutralization of Delta SARS2 virus by boosted mouse sera, as in (A). (**C**) Neutralization of SARS1 pseudovirus (mismatched) by post-boost mouse sera, after immunization with different Quartet and Mosaic immunogens. Dashed horizontal lines represent the limit of detection. The mean is denoted by a bar + 1 s.d., n = 6. * $p < 0.05$, ** $p < 0.01$, *** $p < 0.001$; other comparisons were non-significant.

Quartet Nanocage immunization induces broad antibody responses in animals with a pre-existing focused response

Given the large fraction of the world vaccinated or previously infected with SARS-CoV-2 (671 million confirmed cases and 13 billion vaccine doses administered by February 2023) (*31*, *32*), an outstanding question was whether a broad antibody response could be achieved in the face of a pre-biased immune response. It is not feasible to match the pattern of vaccine sources and timings for different people around the world, but we generated a pre-existing response by priming with SARS2 Wuhan Spike (HexaPro) protein. We then boosted with different immunogens designed to elicit a broad response (Fig. 5A). One hypothesis is that animals with a pre-existing response to SARS2, upon boosting with Quartet Nanocage, would amplify their SARS2 antibodies from a memory response and be less stimulated by other antigens, so the immune response would be narrow. To test this question, we generated Quartet [SARS1], replacing SARS2 with SARS1 RBD (Fig. S5C). This approach led to the ambitious aim of boosting a SARS2 response using an immunogen lacking any SARS2 sequence. We produced Dual Quartet Nanocage [SARS1] by mixing Alternate Quartet and Quartet [SARS1].

Priming with SARS2 Spike raised the expected narrow strain-specific response against SARS2 RBD (Fig. 5B) and negligible response to SARS1 or BtKY72 (Fig. S11). Surprisingly, the different boosts (Fig. 5B) raised similar responses against SARS2, despite SARS2 RBD being absent in Quartet Nanocage [SARS1] and Dual Quartet Nanocage [SARS1] (Fig. 5B). As expected, Quartet Nanocage [SARS1] and Dual Quartet Nanocage [SARS1] raised the strongest response against SARS1 RBD (Fig. 5C). Quartet Nanocage and Mosaic-8 raised greater antibody response than Homotypic Nanocage or Spike boost against SARS1 and BtKY72 (Fig. 5C). Mismatched responses to SARS1 and BtKY72 raised by Mosaic-8 and Quartet Nanocage were similar to the SARS1 response from a single dose of these candidates in naïve mice (Fig. S6B). Together these results demonstrate that Quartet Nanocages achieve broad anti-sarbecovirus response, despite animals being pre-biased in their response to a specific viral antigen. In addition, Quartet Nanocage lacking SARS2 sequences still induces a good level of anti-SARS2 antibodies, while stimulating broad responses across sarbecoviruses.

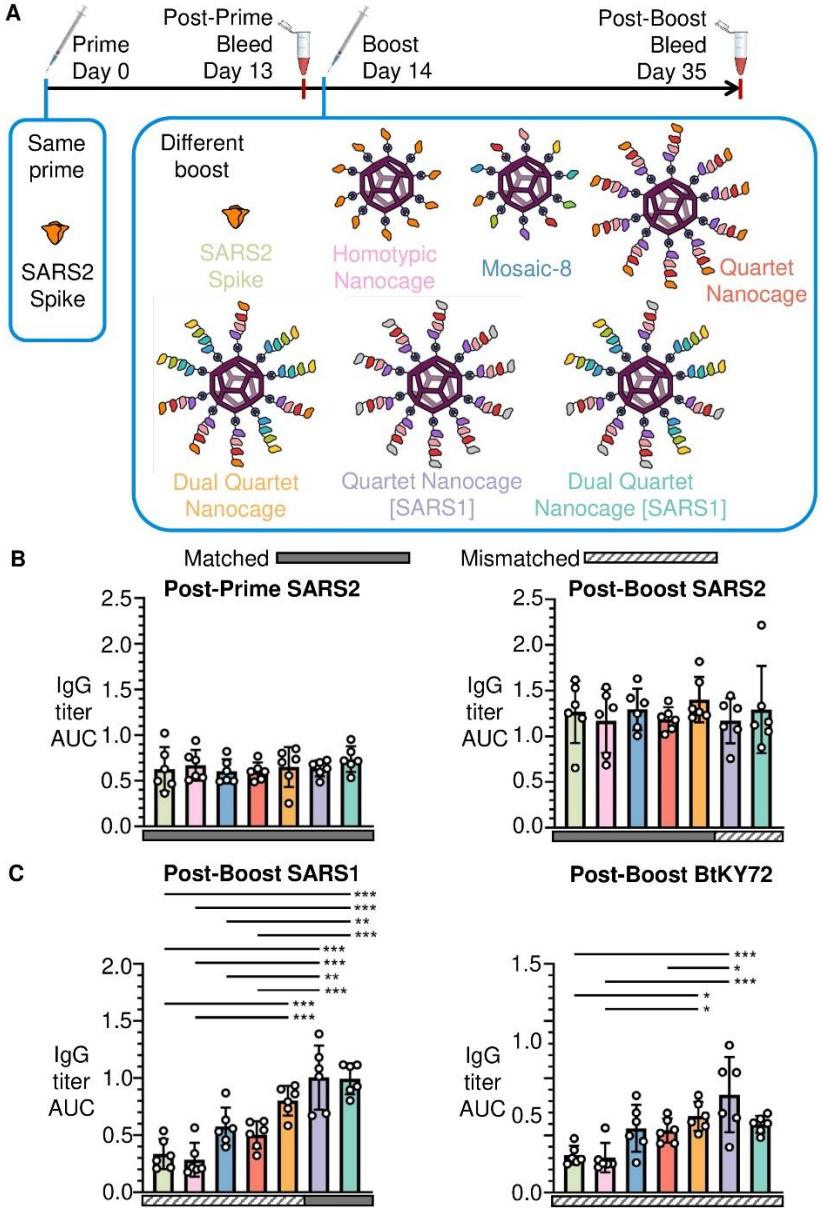

Fig. 5 Quartet immunization induces broad antibodies even after a pre-primed SARS2 response. (**A**) Summary of timeline and antigens for this set of immunizations. (**B**) ELISA for serum IgG to SARS2 RBD presented as the area under the curve of a serial dilution. All mice were primed with Wuhan SARS2 Spike, before boosting with Wuhan SARS2 Spike protein (light green), Homotypic Nanocage (pink), Mosaic-8 (dark blue), SpyTag-Quartet Nanocage (red), Dual Quartet Nanocage (orange), Quartet Nanocage with SARS1 RBD replacing SARS2 (purple), or Dual Quartet Nanocage with SARS1 RBD replacing SARS2 (cyan). Solid rectangles under samples indicate ELISA against a component of that vaccine (matched). Striped rectangles indicate ELISA against an antigen absent in that vaccine (mismatched). Each dot represents one animal. The mean is denoted by a bar ± 1 s.d., n = 6. (**C**) ELISA for serum IgG to other sarbecovirus RBDs, as for (B). * $p < 0.05$, ** $p < 0.01$, *** $p < 0.001$; other comparisons were non-significant.

Discussion

Overall, we have established that RBDs from multiple sarbecoviruses can be efficiently expressed as a tandem construct for assembly onto nanocages, creating a dendritic nanoparticle that elicits neutralizing antibodies against SARS2 variants and diverse other sarbecoviruses. Quartet Nanocage enhanced immune response to antigens present on the nanocage, as well as inducing a high level of antibodies to sarbecovirus antigens absent from the particles. Sequential antigen repeats have mostly been explored for strings of T cell epitopes, where there is no folding to a 3D structure or induction of conformation-sensitive antibodies (*33*). Repeats of related structured domains may challenge the cell's secretion machinery, because of undesired pairings between domains during folding (*34*). However, the cell expression system here efficiently produced the different Quartets that were devised, which may be facilitated by the substantial spacer length and sequence divergence from one domain to the next. In addition, sarbecovirus RBDs exhibit favorable solubility and thermostability (*28*), well suited to advanced antigen assembly strategies.

We were surprised to discover no substantial difference in antibody response to antigens at the start or end of the Quartet. Crystallography or cryoelectron microscopy structures do not allow clear visualization of nanostructures with multiple flexible regions such as the Quartet Nanocage (*35*). Even SpyCatcher003-mi3 coupled to a single SpyTag-RBD showed minimal electron density for RBD in our single-particle cryoelectron microscopy structure (*36*). The glycine/serine linkers between each RBD may provide sufficient flexibility for RBDs near to the nanocage surface to be well exposed to interacting B cells. Upon immunization with Quartet Nanocage, cells with B cell receptors (BCRs) that recognize only a single type of RBD may be less likely to activate efficiently, compared to BCRs recognizing features conserved across sarbecoviruses. Structures have now demonstrated the molecular basis of antibody cross-recognition of diverse sarbecoviruses (*9*, *37–47*). Mosaic-8 design was predicated on the idea that stochastic RBD conjugation is ideal for favoring expansion of cross-reactive B cells. However, Mosaic-8 may face challenges in production and regulatory validation. Here the flexibility of the Quartets may achieve a non-uniform surface for B cell stimulation with a uniformly made immunogen. This arrangement also facilitates a greater number of RBDs to be presented per nanoparticle, which may enhance the amount of antibody induction. The vaccine candidates here employ only two (Quartet Nanocage) or three (Dual Quartet Nanocage) components. Despite this, the levels and breadth of antibodies were at least comparable and in many cases higher than the nine component Mosaic-8.

For many diseases, notably malaria and influenza, vaccines face the challenge of inducing novel protective immunity in people with pre-existing immune responses (*48*, *49*). After priming with SARS2 Wuhan Spike, we found that Quartet Nanocages induced an equivalent level of antibodies against Wuhan RBD as more conventional immunogens (Wuhan Spike or Homotypic SARS2 Nanocages). However, Quartet Nanocages additionally broadened response against diverse sarbecovirus RBDs. These data support that a Quartet Nanocage boost could be effective in a human population with existing focused immunity to SARS2.

Limitations of this study are that we immunized only in mice and that expression of tandem antigens was aided by a robust, monomeric antigen; additional optimization would be required for constructing tandem oligomers of obligate trimeric antigens (*50*). There are differences in the vaccine candidates here compared to Mosaic-8b entering clinical trials:

here antigens were present on the nanocage at sub-saturating levels with SARS2 Wuhan instead of SARS2 Beta RBD.

We detected antibody induction against the nanocage, but data on VLPs decorated using SpyCatcher or genetic fusion indicate that anti-platform antibodies do not impair responses against the target antigen (*51*, *52*). VLP vaccines have generally shown a good safety margin and scalability for cost-effective global production (*14*, *17*). Nonetheless, in future it may be valuable to apply RBD Quartets using viral vectors (*53*) or mRNA vaccines (*54*) and to explore this approach beyond sarbecoviruses, in other alpha/beta-coronaviruses.

SARS-CoV-2 had a devastating medical and societal impact, despite the rapid generation of effective vaccines. Therefore, it is important that vaccinology possesses further improved tools before the next major viral outbreak (*55*, *56*). The generation of Quartet Nanocages that elicit antibodies across a range of viruses may advance proactive vaccinology, in which broadly-protective vaccines are validated before the pandemic danger emerges (*57*).

References

1. J. D. Sachs, S. S. A. Karim, L. Aknin, J. Allen, K. Brosbøl, F. Colombo, G. C. Barron, M. F. Espinosa, V. Gaspar, A. Gaviria, A. Haines, P. J. Hotez, P. Koundouri, F. L. Bascuñán, J.-K. Lee, M. A. Pate, G. Ramos, K. S. Reddy, I. Serageldin, J. Thwaites, V. Vike-Freiberga, C. Wang, M. K. Were, L. Xue, C. Bahadur, M. E. Bottazzi, C. Bullen, G. Laryea-Adjei, Y. B. Amor, O. Karadag, G. Lafortune, E. Torres, L. Barredo, J. G. E. Bartels, N. Joshi, M. Hellard, U. K. Huynh, S. Khandelwal, J. V. Lazarus, S. Michie, The Lancet Commission on lessons for the future from the COVID-19 pandemic. *The Lancet*. **400**, 1224–1280 (2022).

2. S. Iketani, L. Liu, Y. Guo, L. Liu, J. F.-W. Chan, Y. Huang, M. Wang, Y. Luo, J. Yu, H. Chu, K. K.-H. Chik, T. T.-T. Yuen, M. T. Yin, M. E. Sobieszczyk, Y. Huang, K.-Y. Yuen, H. H. Wang, Z. Sheng, D. D. Ho, Antibody evasion properties of SARS-CoV-2 Omicron sublineages. *Nature*. **604**, 553–556 (2022).

3. E. Takashita, S. Yamayoshi, V. Simon, H. van Bakel, E. M. Sordillo, A. Pekosz, S. Fukushi, T. Suzuki, K. Maeda, P. Halfmann, Y. Sakai-Tagawa, M. Ito, S. Watanabe, M. Imai, H. Hasegawa, Y. Kawaoka, Efficacy of Antibodies and Antiviral Drugs against Omicron BA.2.12.1, BA.4, and BA.5 Subvariants. *N Engl J Med*. **387**, 468–470 (2022).

4. E. de Wit, N. van Doremalen, D. Falzarano, V. J. Munster, SARS and MERS: recent insights into emerging coronaviruses. *Nat Rev Microbiol*. **14**, 523–534 (2016).

5. V. D. Menachery, R. L. Graham, R. S. Baric, Jumping species-a mechanism for coronavirus persistence and survival. *Curr Opin Virol*. **23**, 1–7 (2017).

6. A. A. Cohen, P. N. P. Gnanapragasam, Y. E. Lee, P. R. Hoffman, S. Ou, L. M. Kakutani, J. R. Keeffe, H. J. Wu, M. Howarth, A. P. West, C. O. Barnes, M. C. Nussenzweig, P. J. Bjorkman, Mosaic nanoparticles elicit cross-reactive immune responses to zoonotic coronaviruses in mice. *Science*. **371**, 735–741 (2021).

7. T. M. Caradonna, A. G. Schmidt, Protein engineering strategies for rational immunogen design. *npj Vaccines*. **6**, 1–11 (2021).

8. J. Ingale, K. Tran, L. Kong, B. Dey, K. McKee, W. Schief, P. D. Kwong, J. R. Mascola, R. T. Wyatt, Hyperglycosylated Stable Core Immunogens Designed To Present the CD4 Binding Site Are Preferentially Recognized by Broadly Neutralizing Antibodies. *Journal of Virology*. **88**, 14002–14016 (2014).

9. M. E. Abernathy, K.-M. A. Dam, S. R. Esswein, C. A. Jette, P. J. Bjorkman, How Antibodies Recognize Pathogenic Viruses: Structural Correlates of Antibody Neutralization of HIV-1, SARS-CoV-2, and Zika. *Viruses*. **13**, 2106 (2021).

10. L. Dai, L. Gao, L. Tao, S. R. Hadinegoro, M. Erkin, Z. Ying, P. He, R. T. Girsang, H. Vergara, J. Akram, H. I. Satari, T. Khaliq, U. Sughra, A. P. Celi, F. Li, Y. Li, Z. Jiang, D. Dalimova, J. Tuychiev, S. Turdikulova, A. Ikram, N. Flores Lastra, F. Ding, M. Suhardono, E. Fadlyana, J. Yan, Z. Hu, C. Li, I. Y. Abdurakhmonov, G. F. Gao, Efficacy and Safety of the RBD-Dimer–Based Covid-19 Vaccine ZF2001 in Adults. *New England Journal of Medicine*. **386**, 2097–2111 (2022).

11. Y. Liang, J. Zhang, R. Y. Yuan, M. Y. Wang, P. He, J. G. Su, Z. B. Han, Y. Q. Jin, J. W. Hou, H. Zhang, X. F. Zhang, S. Shao, Y. N. Hou, Z. M. Liu, L. F. Du, F. J. Shen, W. M. Zhou, K. Xu, R. Q. Gao, F. Tang, Z. H. Lei, S. Liu, W. Zhen, J. J. Wu, X. Zheng, N. Liu, S. Chen, Z. J. Ma, F. Zheng, S. Y. Ren, Z. Y. Hu, W. J. Huang, G. Z. Wu, C. W. Ke, Q. M. Li, Design of a mutation-integrated trimeric RBD with broad protection against SARS-CoV-2. *Cell Discov*. **8**, 1–17 (2022).

12. D. B. Lee, H. Kim, J. H. Jeong, U. S. Jang, Y. Jang, S. Roh, H. Jeon, E. J. Kim, S. Y. Han, J. Y. Maeng, S. Magez, M. Radwanska, J. Y. Mun, H. S. Jun, G. Lee, M.-S. Song, H.-R. Lee, M. S. Chung, Y. H. Baek, K. H. Kim, Mosaic RBD nanoparticles induce intergenus cross-reactive antibodies and protect against SARS-CoV-2 challenge. *Proceedings of the National Academy of Sciences*. **120**, e2208425120 (2023).

13. M. F. Bachmann, G. T. Jennings, Vaccine delivery: a matter of size, geometry, kinetics and molecular patterns. *Nat Rev Immunol*. **10**, 787-796 (2010).

14. R. A. Hills, M. Howarth, Virus-like particles against infectious disease and cancer: guidance for the nano-architect. *Curr Opin Biotechnol*. **73**, 346–354 (2022).

15. N. C. Dalvie, L. H. Tostanoski, S. A. Rodriguez-Aponte, K. Kaur, S. Bajoria, O. S. Kumru, A. J. Martinot, A. Chandrashekar, K. McMahan, N. B. Mercado, J. Yu, A. Chang, V. M. Giffin, F. Nampanya, S. Patel, L. Bowman, C. A. Naranjo, D. Yun, Z. Flinchbaugh, L. Pessaint, R. Brown, J. Velasco, E. Teow, A. Cook, H. Andersen, M. G. Lewis, D. L. Camp, J. M. Silverman, G. S. Nagar, H. D. Rao, R. R. Lothe, R. Chandrasekharan, M. P. Rajurkar, U. S. Shaligram, H. Kleanthous, S. B. Joshi, D. B. Volkin, S. Biswas, J. C. Love, D. H. Barouch, SARS-CoV-2 receptor binding domain displayed on HBsAg virus–like particles elicits protective immunity in macaques. *Science Advances*. **8**, eabl6015 (2022).

16. S. Preiss, N. Garçon, A. L. Cunningham, R. Strugnell, L. R. Friedland, Vaccine provision: Delivering sustained & widespread use. *Vaccine*. **34**, 6665–6671 (2016).

17. K. A. Collins, R. Snaith, M. G. Cottingham, S. C. Gilbert, A. V. S. Hill, Enhancing protective immunity to malaria with a highly immunogenic virus-like particle vaccine. *Sci Rep*. **7,** 46621 (2017).

18. M. Kanekiyo, M. G. Joyce, R. A. Gillespie, J. R. Gallagher, S. F. Andrews, H. M. Yassine, A. K. Wheatley, B. E. Fisher, D. R. Ambrozak, A. Creanga, K. Leung, E. S. Yang, S. Boyoglu-Barnum, I. S. Georgiev, Y. Tsybovsky, M. S. Prabhakaran, H. Andersen, W.-P. Kong, U. Baxa, K. L. Zephir, J. E. Ledgerwood, R. A. Koup, P. D. Kwong, A. K. Harris, A. B. McDermott, J. R. Mascola, B. S. Graham, Mosaic nanoparticle display of diverse influenza virus hemagglutinins elicits broad B cell responses. *Nat Immunol*. **20**, 362–372 (2019).

19. A. A. Cohen, N. van Doremalen, A. J. Greaney, H. Andersen, A. Sharma, T. N. Starr, J. R. Keeffe, C. Fan, J. E. Schulz, P. N. P. Gnanapragasam, L. M. Kakutani, A. P. West, G. Saturday, Y. E. Lee, H. Gao, C. A. Jette, M. G. Lewis, T. K. Tan, A. R. Townsend, J. D. Bloom, V. J.

Munster, P. J. Bjorkman, Mosaic RBD nanoparticles protect against challenge by diverse sarbecoviruses in animal models. *Science*. **377**, eabq0839 (2022).

20. A. C. Walls, M. C. Miranda, A. Schäfer, M. N. Pham, A. Greaney, P. S. Arunachalam, M.-J. Navarro, M. A. Tortorici, K. Rogers, M. A. O'Connor, L. Shirreff, D. E. Ferrell, J. Bowen, N. Brunette, E. Kepl, S. K. Zepeda, T. Starr, C.-L. Hsieh, B. Fiala, S. Wrenn, D. Pettie, C. Sydeman, K. R. Sprouse, M. Johnson, A. Blackstone, R. Ravichandran, C. Ogohara, L. Carter, S. W. Tilles, R. Rappuoli, S. R. Leist, D. R. Martinez, M. Clark, R. Tisch, D. T. O'Hagan, R. Van Der Most, W. C. Van Voorhis, D. Corti, J. S. McLellan, H. Kleanthous, T. P. Sheahan, K. D. Smith, D. H. Fuller, F. Villinger, J. Bloom, B. Pulendran, R. S. Baric, N. P. King, D. Veesler, Elicitation of broadly protective sarbecovirus immunity by receptor-binding domain nanoparticle vaccines. *Cell*. **184**, 5432-5447.e16 (2021).

21. A. H. Keeble, P. Turkki, S. Stokes, I. N. A. K. Anuar, R. Rahikainen, V. P. Hytonen, M. Howarth, Approaching infinite affinity through engineering of peptide-protein interaction. *Proceedings of the National Academy of Sciences of the United States of America*. **116**, 26523–26533 (2019).

22. Y. Hsia, J. B. Bale, S. Gonen, D. Shi, W. Sheffler, K. K. Fong, U. Nattermann, C. Xu, P.-S. Huang, R. Ravichandran, S. Yi, T. N. Davis, T. Gonen, N. P. King, D. Baker, Design of a hyperstable 60-subunit protein dodecahedron. [corrected]. *Nature*. **535**, 136–139 (2016).

23. T. U. J. Bruun, A. C. Andersson, S. J. Draper, M. Howarth, Engineering a Rugged Nanoscaffold To Enhance Plug-and-Display Vaccination. *ACS Nano*. **12**, 8855–8866 (2018).

24. V. D. Menachery, B. L. Yount, K. Debbink, S. Agnihothram, L. E. Gralinski, J. A. Plante, R. L. Graham, T. Scobey, X.-Y. Ge, E. F. Donaldson, S. H. Randell, A. Lanzavecchia, W. A. Marasco, Z.-L. Shi, R. S. Baric, A SARS-like cluster of circulating bat coronaviruses shows potential for human emergence. *Nat Med*. **21**, 1508–1513 (2015).

25. E. Khaledian, S. Ulusan, J. Erickson, S. Fawcett, M. C. Letko, S. L. Broschat, Sequence determinants of human-cell entry identified in ACE2-independent bat sarbecoviruses: A combined laboratory and computational network science approach. *eBioMedicine*. **79** (2022).

26. T. N. Starr, S. K. Zepeda, A. C. Walls, A. J. Greaney, S. Alkhovsky, D. Veesler, J. D. Bloom, ACE2 binding is an ancestral and evolvable trait of sarbecoviruses. *Nature*. **603**, 913–918 (2022).

27. P. Zhou, X.-L. Yang, X.-G. Wang, B. Hu, L. Zhang, W. Zhang, H.-R. Si, Y. Zhu, B. Li, C.-L. Huang, H.-D. Chen, J. Chen, Y. Luo, H. Guo, R.-D. Jiang, M.-Q. Liu, Y. Chen, X.-R. Shen, X. Wang, X.-S. Zheng, K. Zhao, Q.-J. Chen, F. Deng, L.-L. Liu, B. Yan, F.-X. Zhan, Y.-Y. Wang, G.-F. Xiao, Z.-L. Shi, A pneumonia outbreak associated with a new coronavirus of probable bat origin. *Nature*. **579**, 270–273 (2020).

28. S. K. Vester, R. Rahikainen, I. N. A. Khairil Anuar, R. A. Hills, T. K. Tan, M. Howarth, SpySwitch enables pH- or heat-responsive capture and release for plug-and-display nanoassembly. *Nat Commun*. **13**, 3714 (2022).

29. F. Schmidt, Y. Weisblum, F. Muecksch, H.-H. Hoffmann, E. Michailidis, J. C. C. Lorenzi, P. Mendoza, M. Rutkowska, E. Bednarski, C. Gaebler, M. Agudelo, A. Cho, Z. Wang, A. Gazumyan, M. Cipolla, M. Caskey, D. F. Robbiani, M. C. Nussenzweig, C. M. Rice, T. Hatziioannou, P. D. Bieniasz, Measuring SARS-CoV-2 neutralizing antibody activity using pseudotyped and chimeric viruses. *J Exp Med*. **217**, e20201181 (2020).

30. R. Uraki, M. Ito, Y. Furusawa, S. Yamayoshi, K. Iwatsuki-Horimoto, E. Adachi, M. Saito, M. Koga, T. Tsutsumi, S. Yamamoto, A. Otani, M. Kiso, Y. Sakai-Tagawa, H. Ueki, H.

Yotsuyanagi, M. Imai, Y. Kawaoka, Humoral immune evasion of the omicron subvariants BQ.1.1 and XBB. *The Lancet Infectious Diseases*. **23**, 30–32 (2023).

31. O. J. Watson, G. Barnsley, J. Toor, A. B. Hogan, P. Winskill, A. C. Ghani, Global impact of the first year of COVID-19 vaccination: a mathematical modelling study. *The Lancet Infectious Diseases*. **22**, 1293–1302 (2022).

32. H. Wang, K. R. Paulson, S. A. Pease, S. Watson, H. Comfort, P. Zheng, A. Y. Aravkin, C. Bisignano, R. M. Barber, T. Alam, J. E. Fuller, E. A. May, D. P. Jones, M. E. Frisch, C. Abbafati, C. Adolph, A. Allorant, J. O. Amlag, B. Bang-Jensen, G. J. Bertolacci, S. S. Bloom, A. Carter, E. Castro, S. Chakrabarti, J. Chattopadhyay, R. M. Cogen, J. K. Collins, K. Cooperrider, X. Dai, W. J. Dangel, F. Daoud, C. Dapper, A. Deen, B. B. Duncan, M. Erickson, S. B. Ewald, T. Fedosseeva, A. J. Ferrari, J. J. Frostad, N. Fullman, J. Gallagher, A. Gamkrelidze, G. Guo, J. He, M. Helak, N. J. Henry, E. N. Hulland, B. M. Huntley, M. Kereselidze, A. Lazzar-Atwood, K. E. LeGrand, A. Lindstrom, E. Linebarger, P. A. Lotufo, R. Lozano, B. Magistro, D. C. Malta, J. Månsson, A. M. M. Herrera, F. Marinho, A. H. Mirkuzie, A. T. Misganaw, L. Monasta, P. Naik, S. Nomura, E. G. O'Brien, J. K. O'Halloran, L. T. Olana, S. M. Ostroff, L. Penberthy, R. C. R. Jr, G. Reinke, A. L. P. Ribeiro, D. F. Santomauro, M. I. Schmidt, D. H. Shaw, B. S. Sheena, A. Sholokhov, N. Skhvitaridze, R. J. D. Sorensen, E. E. Spurlock, R. Syailendrawati, R. Topor-Madry, C. E. Troeger, R. Walcott, A. Walker, C. S. Wiysonge, N. A. Worku, B. Zigler, D. M. Pigott, M. Naghavi, A. H. Mokdad, S. S. Lim, S. I. Hay, E. Gakidou, C. J. L. Murray, Estimating excess mortality due to the COVID-19 pandemic: a systematic analysis of COVID-19-related mortality, 2020–21. *The Lancet*. **399**, 1513–1536 (2022).

33. M. Skwarczynski, I. Toth, Peptide-based synthetic vaccines. *Chem Sci*. **7**, 842–854 (2016).

34. A. Borgia, K. R. Kemplen, M. B. Borgia, A. Soranno, S. Shammas, B. Wunderlich, D. Nettels, R. B. Best, J. Clarke, B. Schuler, Transient misfolding dominates multidomain protein folding. *Nat Commun*. **6**, 8861 (2015).

35. M. Palamini, A. Canciani, F. Forneris, Identifying and Visualizing Macromolecular Flexibility in Structural Biology. *Front Mol Biosci*. **3**, 47 (2016).

36. T. K. Tan, P. Rijal, R. Rahikainen, A. H. Keeble, L. Schimanski, S. Hussain, R. Harvey, J. W. P. Hayes, J. C. Edwards, R. K. McLean, V. Martini, M. Pedrera, N. Thakur, C. Conceicao, I. Dietrich, H. Shelton, A. Ludi, G. Wilsden, C. Browning, A. K. Zagrajek, D. Bialy, S. Bhat, P. Stevenson-Leggett, P. Hollinghurst, M. Tully, K. Moffat, C. Chiu, R. Waters, A. Gray, M. Azhar, V. Mioulet, J. Newman, A. S. Asfor, A. Burman, S. Crossley, J. A. Hammond, E. Tchilian, B. Charleston, D. Bailey, T. J. Tuthill, S. P. Graham, H. M. E. Duyvesteyn, T. Malinauskas, J. Huo, J. A. Tree, K. R. Buttigieg, R. J. Owens, M. W. Carroll, R. S. Daniels, J. W. McCauley, D. I. Stuart, K. A. Huang, M. Howarth, A. R. Townsend, A COVID-19 vaccine candidate using SpyCatcher multimerization of the SARS-CoV-2 spike protein receptor-binding domain induces potent neutralising antibody responses. *Nat Commun*. **12**, 542 (2021).

37. J. Huo, Y. Zhao, J. Ren, D. Zhou, H. M. E. Duyvesteyn, H. M. Ginn, L. Carrique, T. Malinauskas, R. R. Ruza, P. N. M. Shah, T. K. Tan, P. Rijal, N. Coombes, K. R. Bewley, J. A. Tree, J. Radecke, N. G. Paterson, P. Supasa, J. Mongkolsapaya, G. R. Screaton, M. Carroll, A. Townsend, E. E. Fry, R. J. Owens, D. I. Stuart, Neutralization of SARS-CoV-2 by Destruction of the Prefusion Spike. *Cell Host & Microbe*. **28**, 445-454.e6 (2020).

38. M. Yuan, D. Huang, C.-C. D. Lee, N. C. Wu, A. M. Jackson, X. Zhu, H. Liu, L. Peng, M. J. van Gils, R. W. Sanders, D. R. Burton, S. M. Reincke, H. Prüss, J. Kreye, D. Nemazee, A. B. Ward, I. A. Wilson, Structural and functional ramifications of antigenic drift in recent SARS-CoV-2 variants. *Science*. **373**, 818–823 (2021).

39. C. A. Jette, A. A. Cohen, P. N. P. Gnanapragasam, F. Muecksch, Y. E. Lee, K. E. Huey-Tubman, F. Schmidt, T. Hatziioannou, P. D. Bieniasz, M. C. Nussenzweig, A. P. West, J. R. Keeffe, P. J. Bjorkman, C. O. Barnes, Broad cross-reactivity across sarbecoviruses exhibited by a subset of COVID-19 donor-derived neutralizing antibodies. *Cell Reports*. **36**, 109760 (2021).

40. M. M. Sauer, M. A. Tortorici, Y.-J. Park, A. C. Walls, L. Homad, O. J. Acton, J. E. Bowen, C. Wang, X. Xiong, W. de van der Schueren, J. Quispe, B. G. Hoffstrom, B.-J. Bosch, A. T. McGuire, D. Veesler, Structural basis for broad coronavirus neutralization. *Nat Struct Mol Biol*. **28**, 478–486 (2021).

41. T. N. Starr, N. Czudnochowski, Z. Liu, F. Zatta, Y.-J. Park, A. Addetia, D. Pinto, M. Beltramello, P. Hernandez, A. J. Greaney, R. Marzi, W. G. Glass, I. Zhang, A. S. Dingens, J. E. Bowen, M. A. Tortorici, A. C. Walls, J. A. Wojcechowskyj, A. De Marco, L. E. Rosen, J. Zhou, M. Montiel-Ruiz, H. Kaiser, J. R. Dillen, H. Tucker, J. Bassi, C. Silacci-Fregni, M. P. Housley, J. di Iulio, G. Lombardo, M. Agostini, N. Sprugasci, K. Culap, S. Jaconi, M. Meury, E. Dellota Jr, R. Abdelnabi, S.-Y. C. Foo, E. Cameroni, S. Stumpf, T. I. Croll, J. C. Nix, C. Havenar-Daughton, L. Piccoli, F. Benigni, J. Neyts, A. Telenti, F. A. Lempp, M. S. Pizzuto, J. D. Chodera, C. M. Hebner, H. W. Virgin, S. P. J. Whelan, D. Veesler, D. Corti, J. D. Bloom, G. Snell, SARS-CoV-2 RBD antibodies that maximize breadth and resistance to escape. *Nature*. **597**, 97–102 (2021).

42. D. R. Martinez, A. Schäfer, S. Gobeil, D. Li, G. De la Cruz, R. Parks, X. Lu, M. Barr, V. Stalls, K. Janowska, E. Beaudoin, K. Manne, K. Mansouri, R. J. Edwards, K. Cronin, B. Yount, K. Anasti, S. A. Montgomery, J. Tang, H. Golding, S. Shen, T. Zhou, P. D. Kwong, B. S. Graham, J. R. Mascola, D. C. Montefiori, S. M. Alam, G. D. Sempowski, S. Khurana, K. Wiehe, K. O. Saunders, P. Acharya, B. F. Haynes, R. S. Baric, A broadly cross-reactive antibody neutralizes and protects against sarbecovirus challenge in mice. *Science Translational Medicine*. **14**, eabj7125 (2021).

43. C. Fan, A. A. Cohen, M. Park, A. F.-H. Hung, J. R. Keeffe, P. N. P. Gnanapragasam, Y. E. Lee, H. Gao, L. M. Kakutani, Z. Wu, H. Kleanthous, K. E. Malecek, J. C. Williams, P. J. Bjorkman, Neutralizing monoclonal antibodies elicited by mosaic RBD nanoparticles bind conserved sarbecovirus epitopes. *Immunity*. **55**, 2419-2435.e10 (2022).

44. C. G. Rappazzo, L. V. Tse, C. I. Kaku, D. Wrapp, M. Sakharkar, D. Huang, L. M. Deveau, T. J. Yockachonis, A. S. Herbert, M. B. Battles, C. M. O'Brien, M. E. Brown, J. C. Geoghegan, J. Belk, L. Peng, L. Yang, Y. Hou, T. D. Scobey, D. R. Burton, D. Nemazee, J. M. Dye, J. E. Voss, B. M. Gunn, J. S. McLellan, R. S. Baric, L. E. Gralinski, L. M. Walker, Broad and potent activity against SARS-like viruses by an engineered human monoclonal antibody. *Science*. **371**, 823–829 (2021).

45. W. He, R. Musharrafieh, G. Song, K. Dueker, L. V. Tse, D. R. Martinez, A. Schäfer, S. Callaghan, P. Yong, N. Beutler, J. L. Torres, R. M. Volk, P. Zhou, M. Yuan, H. Liu, F. Anzanello, T. Capozzola, M. Parren, E. Garcia, S. A. Rawlings, D. M. Smith, I. A. Wilson, Y. Safonova, A. B. Ward, T. F. Rogers, R. S. Baric, L. E. Gralinski, D. R. Burton, R. Andrabi, Targeted isolation of panels of diverse human protective broadly neutralizing antibodies against SARS-like viruses. *Nature Immunology*. **23**, 960–970 (2022).

46. Y.-J. Park, A. De Marco, T. N. Starr, Z. Liu, D. Pinto, A. C. Walls, F. Zatta, S. K. Zepeda, J. E. Bowen, K. R. Sprouse, A. Joshi, M. Giurdanella, B. Guarino, J. Noack, R. Abdelnabi, S.-Y. C. Foo, L. E. Rosen, F. A. Lempp, F. Benigni, G. Snell, J. Neyts, S. P. J. Whelan, H. W. Virgin, J. D. Bloom, D. Corti, M. S. Pizzuto, D. Veesler, Antibody-mediated broad sarbecovirus neutralization through ACE2 molecular mimicry. *Science*. **375**, 449–454 (2022).

47. K.-Y. A. Huang, X. Chen, A. Mohapatra, H. T. V. Nguyen, L. Schimanski, T. K. Tan, P. Rijal, S. K. Vester, R. A. Hills, M. Howarth, J. R. Keeffe, A. A. Cohen, L. M. Kakutani, Y.-M. Wu, M. Shahed-Al-Mahmud, Y.-C. Chou, P. J. Bjorkman, A. R. Townsend, C. Ma, Structural basis

for a conserved neutralization epitope on the receptor-binding domain of SARS-CoV-2. *Nat Commun*. **14**, 311 (2023).

48. T. J. Owalla, D. E. B. Hergott, A. M. Seilie, W. Staubus, C. Chavtur, M. Chang, J. G. Kublin, T. G. Egwang, S. C. Murphy, Rethinking detection of pre-existing and intervening Plasmodium infections in malaria clinical trials. *Front Immunol*. **13**, 1003452 (2022).

49. M. Knight, S. Changrob, L. Li, P. C. Wilson, Imprinting, immunodominance, and other impediments to generating broad influenza immunity. *Immunol Rev*. **296**, 191–204 (2020).

50. R. Rahikainen, P. Rijal, T. K. Tan, H. J. Wu, A. C. Andersson, J. R. Barrett, T. A. Bowden, S. J. Draper, A. R. Townsend, M. Howarth, Overcoming Symmetry Mismatch in Vaccine Nanoassembly through Spontaneous Amidation. *Angew Chem Int Ed Engl*. **60**, 321-330 (2021).

51. A. Marini, Y. Zhou, Y. Li, I. J. Taylor, D. B. Leneghan, J. Jin, M. Zaric, D. Mekhaiel, C. A. Long, K. Miura, S. Biswas, A Universal Plug-and-Display Vaccine Carrier Based on HBsAg VLP to Maximize Effective Antibody Response. *Front Immunol*. **10**, 2931 (2019).

52. J. C. Kraft, M. N. Pham, L. Shehata, M. Brinkkemper, S. Boyoglu-Barnum, K. R. Sprouse, A. C. Walls, S. Cheng, M. Murphy, D. Pettie, M. Ahlrichs, C. Sydeman, M. Johnson, A. Blackstone, D. Ellis, R. Ravichandran, B. Fiala, S. Wrenn, M. Miranda, K. Sliepen, P. J. M. Brouwer, A. Antanasijevic, D. Veesler, A. B. Ward, M. Kanekiyo, M. Pepper, R. W. Sanders, N. P. King, Antigen- and scaffold-specific antibody responses to protein nanoparticle immunogens. *Cell Rep Med*. **3**, 100780 (2022).

53. M. D. J. Dicks, L. M. Rose, R. A. Russell, L. A. H. Bowman, C. Graham, J. M. Jimenez-Guardeño, K. J. Doores, M. H. Malim, S. J. Draper, M. Howarth, S. Biswas, Modular capsid decoration boosts adenovirus vaccine-induced humoral immunity against SARS-CoV-2. *Molecular Therapy*. **30**, 3639–3657 (2022).

54. Z. Zhang, J. Mateus, C. H. Coelho, J. M. Dan, C. R. Moderbacher, R. I. Gálvez, F. H. Cortes, A. Grifoni, A. Tarke, J. Chang, E. A. Escarrega, C. Kim, B. Goodwin, N. I. Bloom, A. Frazier, D. Weiskopf, A. Sette, S. Crotty, Humoral and cellular immune memory to four COVID-19 vaccines. *Cell*. **185**, 2434-2451.e17 (2022).

55. J. A. Lednicky, M. S. Tagliamonte, S. K. White, M. A. Elbadry, M. M. Alam, C. J. Stephenson, T. S. Bonny, J. C. Loeb, T. Telisma, S. Chavannes, D. A. Ostrov, C. Mavian, V. M. Beau De Rochars, M. Salemi, J. G. Morris, Independent infections of porcine deltacoronavirus among Haitian children. *Nature*. **600**, 133–137 (2021).

56. A. N. Vlasova, A. Diaz, D. Damtie, L. Xiu, T.-H. Toh, J. S.-Y. Lee, L. J. Saif, G. C. Gray, Novel Canine Coronavirus Isolated from a Hospitalized Patient With Pneumonia in East Malaysia. *Clin Infect Dis*. **74**, 446–454 (2022).

57. M. Saville, J. P. Cramer, M. Downham, A. Hacker, N. Lurie, L. Van der Veken, M. Whelan, R. Hatchett, Delivering Pandemic Vaccines in 100 Days — What Will It Take? *New England Journal of Medicine*. **387**, e3 (2022).

58. B. Zakeri, J. O. Fierer, E. Celik, E. C. Chittock, U. Schwarz-Linek, V. T. Moy, M. Howarth, Peptide tag forming a rapid covalent bond to a protein, through engineering a bacterial adhesin. *Proceedings of the National Academy of Sciences*. **109**, 690-697 (2012).

59. C.-L. Hsieh, J. A. Goldsmith, J. M. Schaub, A. M. DiVenere, H.-C. Kuo, K. Javanmardi, K. C. Le, D. Wrapp, A. G. Lee, Y. Liu, C.-W. Chou, P. O. Byrne, C. K. Hjorth, N. V. Johnson, J. Ludes-Meyers, A. W. Nguyen, J. Park, N. Wang, D. Amengor, J. J. Lavinder, G. C. Ippolito, J. A. Maynard, I. J. Finkelstein, J. S. McLellan, Structure-based design of prefusion-stabilized SARS-CoV-2 spikes. *Science*. **369**, 1501–1505 (2020).

60. Y. Aida, M. J. Pabst, Removal of endotoxin from protein solutions by phase separation using Triton X-114. *J Immunol Methods*. **132**, 191–195 (1990).

61. K. D. Brune, D. B. Leneghan, I. J. Brian, A. S. Ishizuka, M. F. Bachmann, S. J. Draper, S. Biswas, M. Howarth, Plug-and-Display: decoration of Virus-Like Particles via isopeptide bonds for modular immunization. *Sci Rep*. **6**, 19234 (2016).

62. L. A. Brito, M. Singh, Acceptable levels of endotoxin in vaccine formulations during preclinical research. *J Pharm Sci*. **100**, 34–37 (2011).

63. P. Virtanen, R. Gommers, T. E. Oliphant, M. Haberland, T. Reddy, D. Cournapeau, E. Burovski, P. Peterson, W. Weckesser, J. Bright, S. J. van der Walt, M. Brett, J. Wilson, K. J. Millman, N. Mayorov, A. R. J. Nelson, E. Jones, R. Kern, E. Larson, C. J. Carey, İ. Polat, Y. Feng, E. W. Moore, J. VanderPlas, D. Laxalde, J. Perktold, R. Cimrman, I. Henriksen, E. A. Quintero, C. R. Harris, A. M. Archibald, A. H. Ribeiro, F. Pedregosa, P. van Mulbregt, SciPy 1.0 Contributors, SciPy 1.0: fundamental algorithms for scientific computing in Python. *Nat Methods*. **17**, 261–272 (2020).

64. C. R. Harris, K. J. Millman, S. J. van der Walt, R. Gommers, P. Virtanen, D. Cournapeau, E. Wieser, J. Taylor, S. Berg, N. J. Smith, R. Kern, M. Picus, S. Hoyer, M. H. van Kerkwijk, M. Brett, A. Haldane, J. F. del Río, M. Wiebe, P. Peterson, P. Gérard-Marchant, K. Sheppard, T. Reddy, W. Weckesser, H. Abbasi, C. Gohlke, T. E. Oliphant, Array programming with NumPy. *Nature*. **585**, 357–362 (2020).

65. H. Hartman, Y. Wang, H. W. Schroeder, X. Cui, Absorbance summation: A novel approach for analyzing high-throughput ELISA data in the absence of a standard. *PLoS One*. **13**, e0198528 (2018).

66. L. Caly, J. Druce, J. Roberts, K. Bond, T. Tran, R. Kostecki, Y. Yoga, W. Naughton, G. Taiaroa, T. Seemann, M. B. Schultz, B. P. Howden, T. M. Korman, S. R. Lewin, D. A. Williamson, M. G. Catton, Isolation and rapid sharing of the 2019 novel coronavirus (SARS-CoV-2) from the first patient diagnosed with COVID-19 in Australia. *Medical Journal of Australia*. **212**, 459–462 (2020).

67. S. Cele, I. Gazy, L. Jackson, S.-H. Hwa, H. Tegally, G. Lustig, J. Giandhari, S. Pillay, E. Wilkinson, Y. Naidoo, F. Karim, Y. Ganga, K. Khan, M. Bernstein, A. B. Balazs, B. I. Gosnell, W. Hanekom, M.-Y. S. Moosa, R. J. Lessells, T. de Oliveira, A. Sigal, Escape of SARS-CoV-2 501Y.V2 from neutralization by convalescent plasma. *Nature*. **593**, 142–146 (2021).

68. K.-Y. A. Huang, T. K. Tan, T.-H. Chen, C.-G. Huang, R. Harvey, S. Hussain, C.-P. Chen, A. Harding, J. Gilbert-Jaramillo, X. Liu, M. Knight, L. Schimanski, S.-R. Shih, Y.-C. Lin, C.-Y. Cheng, S.-H. Cheng, Y.-C. Huang, T.-Y. Lin, J.-T. Jan, C. Ma, W. James, R. S. Daniels, J. W. McCauley, P. Rijal, A. R. Townsend, Breadth and function of antibody response to acute SARS-CoV-2 infection in humans. *PLoS Pathog*. **17**, e1009352 (2021).

69. K. H. D. Crawford, R. Eguia, A. S. Dingens, A. N. Loes, K. D. Malone, C. R. Wolf, H. Y. Chu, M. A. Tortorici, D. Veesler, M. Murphy, D. Pettie, N. P. King, A. B. Balazs, J. D. Bloom, Protocol and Reagents for Pseudotyping Lentiviral Particles with SARS-CoV-2 Spike Protein for Neutralization Assays. *Viruses*. **12**, 513 (2020).

70. D. F. Robbiani, C. Gaebler, F. Muecksch, J. C. C. Lorenzi, Z. Wang, A. Cho, M. Agudelo, C. O. Barnes, A. Gazumyan, S. Finkin, T. Hägglöf, T. Y. Oliveira, C. Viant, A. Hurley, H.-H. Hoffmann, K. G. Millard, R. G. Kost, M. Cipolla, K. Gordon, F. Bianchini, S. T. Chen, V. Ramos, R. Patel, J. Dizon, I. Shimeliovich, P. Mendoza, H. Hartweger, L. Nogueira, M. Pack, J. Horowitz, F. Schmidt, Y. Weisblum, E. Michailidis, A. W. Ashbrook, E. Waltari, J. E. Pak, K. E. Huey-Tubman, N. Koranda, P. R. Hoffman, A. P. West, C. M. Rice, T. Hatziioannou, P. J.

Bjorkman, P. D. Bieniasz, M. Caskey, M. C. Nussenzweig, Convergent antibody responses to SARS-CoV-2 in convalescent individuals. *Nature*. **584**, 437–442 (2020).

71. A. P. West, L. Scharf, J. Horwitz, F. Klein, M. C. Nussenzweig, P. J. Bjorkman, Computational analysis of anti–HIV-1 antibody neutralization panel data to identify potential functional epitope residues. *Proceedings of the National Academy of Sciences*. **110**, 10598–10603 (2013).

72. K. Tamura, G. Stecher, S. Kumar, MEGA11: Molecular Evolutionary Genetics Analysis Version 11. *Molecular Biology and Evolution*. **38**, 3022–3027 (2021).

73. F. Madeira, Y. mi Park, J. Lee, N. Buso, T. Gur, N. Madhusoodanan, P. Basutkar, A. R. N. Tivey, S. C. Potter, R. D. Finn, R. Lopez, The EMBL-EBI search and sequence analysis tools APIs in 2019. *Nucleic Acids Research*. **47**, W636–W641 (2019).

74. D. Zhou, H. M. E. Duyvesteyn, C.-P. Chen, C.-G. Huang, T.-H. Chen, S.-R. Shih, Y.-C. Lin, C.-Y. Cheng, S.-H. Cheng, Y.-C. Huang, T.-Y. Lin, C. Ma, J. Huo, L. Carrique, T. Malinauskas, R. R. Ruza, P. N. M. Shah, T. K. Tan, P. Rijal, R. F. Donat, K. Godwin, K. R. Buttigieg, J. A. Tree, J. Radecke, N. G. Paterson, P. Supasa, J. Mongkolsapaya, G. R. Screaton, M. W. Carroll, J. Gilbert-Jaramillo, M. L. Knight, W. James, R. J. Owens, J. H. Naismith, A. R. Townsend, E. E. Fry, Y. Zhao, J. Ren, D. I. Stuart, K.-Y. A. Huang, Structural basis for the neutralization of SARS-CoV-2 by an antibody from a convalescent patient. *Nat Struct Mol Biol*. **27**, 950–958 (2020).

Acknowledgements

We thank Dr. David Staunton from the University of Oxford Department of Biochemistry Biophysical Suite for help with biophysical analysis. We thank the Centre for the AIDS Programme of Research in South Africa (CAPRISA) and Gavin Screaton (University of Oxford) for supplying SARS-CoV-2 variant isolates. The BtKY72 K493Y/T498W Spike plasmid for generating pseudovirus was a kind gift to the Bjorkman lab from David Veesler (University of Washington).

Funding: Funding for this study was provided by:
Biotechnology and Biological Sciences Research Council (BBSRC BB/S007369/1) (A.H.K. and M.H.);
Rhodes Trust (R.H.);
EPA Cephalosporin Early Career Teaching and Research Fellowship (T.K.T.);
Townsend-Jeantet Prize Charitable Trust (Charity Number 1011770) (T.K.T.);
Chinese Academy of Medical Sciences (CAMS) Innovation Fund for Medical Science (CIFMS), China (grant no. 2018-I2M-2-002) (A.R.T.);
University of Oxford COVID-19 Research Response Fund and its donors (reference 0009517) (M.H.)
National Institutes of Health (NIH) NIH AI165075 (P.J.B.);
Caltech Merkin Institute (P.J.B.);
George Mason University Fast Grant (P.J.B.).

Author Contributions: R.A.H. performed all experiments except T.K.T. performed mouse immunizations, J.R.K., P.N.P.G. and K.N.S. tested pseudovirus neutralization, and W.S.J., M.L.H., S.L., J.G-J., M.A. and A.N. tested virus neutralization. A.H.K. designed and purified initial Quartet constructs. R.A.H., T.T., A.A.C., W.S.J., P.J.B., A.R.T. and M.H. designed the project. R.A.H. and M.H. wrote the manuscript. All authors read and approved the manuscript.

Competing interests: M.H. is an inventor on a patent on spontaneous amide bond formation (EP2534484) and a SpyBiotech co-founder and shareholder. M.H. and A.H.K. are inventors on a patent on SpyTag003:SpyCatcher003 (UK Intellectual Property Office 1706430.4). P.J.B. and A.A.C. are inventors on a US patent application filed by the California Institute of Technology that covers the methodology to generate cross-reactive antibodies using mosaic nanoparticles. P.J.B., and A.A.C. are inventors on a US patent application filed by the California Institute of Technology that covers the monoclonal antibodies elicited by vaccination with Mosaic nanoparticles described in this work. P.J.B., A.A.C. and J.R.K. are inventors on a US patent application filed by the California Institute of Technology that covers the methods of isolating cross-reactive antibodies by vaccination with mosaic nanoparticles. All other authors have no competing interests to declare.

Data availability: Sequences of constructs are available in GenBank, as described in the section "Plasmids and Cloning". Plasmids encoding pDEST14-SpySwitch, pET28a-SpyCatcher003-mi3, pET28a-SpyTag-MBP, pcDNA3.1-SpyTag-Quartet, pcDNA3.1-Alternate Quartet and pcDNA3.1-Quartet [SARS1] will be deposited before publication in the Addgene repository (https://www.addgene.org/Mark_Howarth/). Further information and request for resources and reagents should be directed to and will be fulfilled by the lead contact, M.H. (mh2186@cam.ac.uk).

Supplementary Materials

Materials and Methods
Figs. S1 to S11

SUPPLEMENTARY MATERIALS

Materials and Methods
Figs. S1 to S11

Materials and Methods

Plasmids and Cloning

Cloning was performed using standard PCR methods with Q5 High-Fidelity 2× Master Mix (New England Biolabs) and Gibson assembly. All open-reading frames were validated by Sanger sequencing (Source Bioscience).

pET28a-SpyCatcher003-mi3 (GenBank MT945417, Addgene 159995) was previously described (*50*). pET28a-SpyTag-MBP (GenBank MQ038699, Addgene 35050) has been published (*58*). pDEST14-SpySwitch (GenBank ON131074, Addgene plasmid ID 184225) was previously described (*28*). Monomeric sarbecovirus RBD expression vectors contained a C-terminal SpyTag003 (RGVPHIVMVDAYKRYK) (*21*) and His_8-tag (*6*) in the plasmid p3BNC-RBD-His8-SpyTag003 and were previously described (*28*): SARS-CoV-2 (GenBank ON131086), SARS-CoV (GenBank ON131087), RaTG13-CoV (GenBank ON131088), SHC014-CoV (GenBank ON131089), Rs4081-CoV (GenBank ON131090), pangolin17 (pang17)-CoV (GenBank ON131091), RmYN02-CoV (GenBank ON131092), Rf1-CoV (GenBank ON131093), WIV1-CoV (GenBank ON131094), Yunnan2011 (Yun11)-CoV (GenBank ON131095), BM-4831-CoV (GenBank ON131096), and BtKY72-CoV (GenBank ON131097)]. The origins of the sarbecovirus RBDs are SARS1 (GenBank AAP13441.1; residues 318-510), WIV1 (GenBank KF367457; residues 307-528), SHC014 (GenBank KC881005; residues 307-524), BM-4831 (GenBank NC014470; residues 310-530), BtKY72 (GenBank KY352407; residues 309-530), pang17 (GenBank QIA48632; residues 317-539), SARS2 (GenBank NC045512; S protein residues 331–529), RaTG13 (GenBank QHR63300; S protein residues 319-541), Rs4081 (GenBank KY417143; S protein residues 310-515), RmYN02 (GSAID EPI_ISL_412977; residues 298-503), and Rf1 (GenBank DQ412042; residues 310-515). The SARS2 Wuhan Spike protein was the HexaPro variant (a gift from Jason McLellan, Addgene plasmid ID 154754) that contains six proline substitutions (F817P, A892P, A899P, A942P, K986P, V987P) that confer greater stability and has been previously described (*59*). The SARS2 Beta variant Spike protein was cloned from HexaPro to match the B.1.351 variant (L18F, D80A, D215G, Δ242-244, R246I, K417N, E484K, N501Y, D614G, A701V) in addition to the previously outlined six proline mutations. The SARS2 Delta variant Spike protein was cloned from HexaPro to match the B.1.617.2 variant (T19R, T95I, G142D, Δ156-157, R158G, L452R, T478K, D614G, P681R, D950N) in addition to the previously outlined six proline mutations.

Quartet RBD constructs were cloned in competent *E. coli* DH5α cells and began with the influenza H7 hemagglutinin (A/HongKong/125/2017) signal-peptide sequence. Each RBD was separated with an 8 or 9 residue Gly-Ser linker that was unique within the construct. pcDNA3.1-Quartet-SpyTag was created by cloning from the N-terminus to C-terminus SHC014 RBD, Rs4081 RBD, RaTG13 RBD and SARS2 RBD with a C-terminal SpyTag into pcDNA3.1 (Fig. 1C, GenBank and Addgene deposition in progress). This is the construct used for Fig. 1 and 2. For subsequent figures, pcDNA3.1-SpyTag-Quartet was cloned with a SpyTag after the signal sequence and then the same order of RBDs (SpyTag-SHC014-Rs4081-RaTG13-SARS2) (Fig. S5, GenBank and Addgene deposition in progress). pcDNA3.1-Quartet [SARS1] was cloned with SpyTag after the signal sequence, with SARS1 in the position of SARS2 (SpyTag-SHC014-Rs4081-RaTG13-SARS1) (Fig. S5, GenBank

and Addgene deposition in progress). pcDNA3.1-Alternate Quartet was cloned with SpyTag after the signal sequence, followed by pang17 RBD, RmYN02 RBD, Rf1 RBD, and WIV1 RBD (Fig. S5, GenBank and Addgene deposition in progress).

Bacterial Expression

pET28a-SpyCatcher003-mi3 or pET28a-SpyTag-MBP were transformed into *E. coli* BL21(DE3) cells (Agilent) and grown on LB-Agar plates with 50 µg/mL kanamycin for 16 h at 37 °C. A single colony was added in 10 mL LB medium containing 50 µg/mL kanamycin and grown for 16 h at 37 °C with shaking at 200 rpm. This starter culture was then added to 1 L LB containing 50 µg/mL kanamycin and incubated at 37 °C and 200 rpm shaking until OD_{600} 0.6. Cultures were induced with 0.5 mM isopropyl β-D-1-thiogalactopyranoside (IPTG). For SpyCatcher003-mi3, cells were grown at 22 °C with shaking at 200 rpm for 16 h. For SpyTag-MBP, cells were grown at 30 °C with shaking at 200 rpm for 4 h. Cultures were pelleted by centrifugation at 4,000 g.

Purification of SpyCatcher003-mi3

Cell pellets were resuspended in 20 mL 20 mM Tris-HCl, 300 mM NaCl, pH 8.5 supplemented with 0.1 mg/mL lysozyme, 1 mg/mL cOmplete mini EDTA-free protease inhibitor (Roche) and 1 mM phenylmethanesulfonyl fluoride (PMSF). The lysate was incubated at 4 °C for 45 min with end-over-end mixing. An Ultrasonic Processor equipped with a microtip (Cole-Parmer) was used to perform sonication on ice (4 times for 60 s, 50% duty-cycle). Centrifugation at 35,000 g for 45 min at 4 °C was used to clear cell debris. 170 mg of ammonium sulfate was added per mL of lysate and incubated at 4 °C for 1 h, while mixing at 120 rpm to precipitate the particles. The solution was centrifuged for 30 min at 30,000 g at 4 °C. The pellet was resuspended in 10 mL mi3 buffer (25 mM Tris–HCl, 150 mM NaCl, pH 8.0) at 4 °C and filtered sequentially through 0.45 µm and 0.22 µm syringe filters (Starlab). The filtrate was dialyzed for 16 h against 1,000-fold excess mi3 buffer. The dialyzed particles were centrifuged at 17,000 g for 30 min at 4 °C and filtered through a 0.22 µm syringe filter. The purified SpyCatcher003-mi3 was loaded onto a HiPrep Sephacryl S-400 HR 16-600 column (GE Healthcare), which was equilibrated with mi3 buffer using an ÄKTA Pure 25 system (GE Healthcare). The proteins were separated at 0.1 mL/min while collecting 1 mL elution factions. The fractions containing the purified particles were pooled and concentrated using a Vivaspin 20 100 kDa molecular weight cut-off centrifugal concentrator (GE Healthcare) and stored at −80 °C.

Mammalian Protein Expression

Mammalian expression of all RBD and Spike constructs was performed in Expi293F cells (Thermo Fisher, A14635). Expi293F cells were grown under humidified conditions at 37 °C and 8% (v/v) CO_2 in Expi293 Expression Medium (Thermo Fisher) with 50 U/mL penicillin and 50 µg/mL streptomycin. Transfections were performed using the ExpiFectamine 293 Transfection Kit (Thermo Fisher). Expi293F cells were brought to 3×10^6 cells/mL and then 1 µg plasmid DNA per mL culture was incubated with ExpiFectamine 293 reagent for 20 min, before being added dropwise to the Expi293F culture. After approximately 20 h, ExpiFectamine 293 Transfection Enhancers 1 and 2 were added. Cell supernatants were harvested after 5 days by centrifuging for 4,000 g at 4 °C for 5 min and were passed through a 0.45 µm filter and then a 0.22 µm filter (Starlab).

SpySwitch Purification

RBDs, Quartets and SpyTag-MBP were purified by SpySwitch (*28*). Purifications were performed at 4 °C. For SpyTag-MBP, cells were lysed according to the same procedure as

SpyCatcher003-mi3 and supplemented with 10× SpySwitch buffer (500 mM Tris-HCl pH 7.5 + 3 M NaCl) 10% (v/v). For mammalian proteins, 10 × SpySwitch buffer was added to mammalian culture supernatant at 10% (v/v). SpySwitch resin (*28*), packed in an Econo-Pac Chromatography Column (Bio-Rad), was pre-equilibrated with 2 × 10 column volumes (CV) of SpySwitch buffer (50 mM Tris-HCl pH 7.5 + 300 mM NaCl). The supernatant was incubated with SpySwitch resin for 1 h at 4 °C on an end-over-end rotator. The column was washed twice with 15 CV SpySwitch buffer. Proteins were eluted using a weakly acidic pH switch. The protein was incubated with 1.5 CV of SpySwitch Elution Buffer (50 mM acetic acid/sodium acetate pH 5.0 + 150 mM NaCl) at 4 °C with the column capped. The cap was removed and the elution flow-through was collected into a microcentrifuge tube containing 0.3 CV 1 M Tris-HCl pH 8.0. The microcentrifuge tube was mixed by inversion to minimize the time spent at an acidic pH. This elution step was repeated for a total of six times. Purification was assessed by SDS-PAGE with Coomassie staining. Briefly, 10 µL of fractions were mixed with 2 µL 6× SDS loading buffer [234 mM Tris-HCl pH 6.8, 24% (v/v) glycerol, 120 µM bromophenol blue, 234 mM SDS], before heating at 95 °C for 5 min in a C1000 Touch Thermal Cycler (Bio-Rad) and loading onto 12% SDS-PAGE, before staining with Coomassie. Typical yields for the RBD Quartets are 50-75 mg per L of culture. Typical yields for RBD monomers were 80-160 mg per L of culture, as measured by bicinchoninic acid (BCA). Elution fractions were dialyzed for 16 h against 1,000-fold excess Tris-buffered saline (TBS: 50 mM Tris-HCl, 150 mM NaCl, pH 7.4 at 25 °C). Proteins were stored in aliquots at -80 °C.

Ni-NTA Purification

SARS-CoV-2 Spike proteins were purified by nickel-nitrilotriacetic acid (Ni-NTA) affinity chromatography. Mammalian supernatants were supplemented with 10× Ni-NTA buffer (500 mM Tris-HCl, 3 M NaCl, pH 7.8) at 10% (v/v). Ni-NTA agarose (Qiagen) was packed in an Econo-Pac Chromatography Column (Bio-Rad) and washed with 2 × 10 CV of Ni-NTA buffer (50 mM Tris-HCl, 300 mM NaCl, pH 7.8). Mammalian supernatant was incubated in the Ni-NTA column for 1 h at 4 °C with rolling. The supernatant was allowed to flow through by gravity, before being washed with 2 × 10 CV of Ni-NTA wash buffer (10 mM imidazole in Ni-NTA buffer). Elutions were performed by incubating resin with Ni-NTA elution buffer (200 mM imidazole in Ni-NTA buffer) for 5 min, before eluting by gravity. A total of six 1 CV elutions were performed. Elution fractions were assessed by SDS-PAGE with Coomassie staining, pooled, and dialyzed for 16 h against 1,000-fold excess TBS.

PNGase F Digestion

Quartet protein (2 µg) was incubated with 1 µL Glycoprotein Denaturing Buffer (10×) (New England Biolabs) at 100 °C for 10 min with a C1000 Touch Thermal Cycler (Bio-Rad). The denatured protein was then chilled on ice for 1 min and centrifuged for 10 s at 2,000 g with a MiniStar silverline (VWR). Then 2 µL GlycoBuffer 2 (10×) (New England Biolabs), 2 µL 10% (v/v) NP-40, 6 µL MilliQ water and 1 µL PNGase F (New England Biolabs) at 500,000 units/mL were added and incubated at 37 °C for 1 h. Proteins were resolved on 12% SDS-PAGE, stained with Coomassie, and imaged using a ChemiDoc XRS imager.

Dynamic Light Scattering (DLS)

2 µM SpyTag-antigens were conjugated with 2 µM SpyCatcher003-mi3 for 48 h at 4 °C. Proteins were centrifuged for 30 min at 16,900 g at 4 °C and 30 µL of the supernatant was loaded into a quartz cuvette. Samples were measured at 20 °C using a Viscotek 802 (Viscotek) with 20 scans of 10 s each, using 50% laser intensity, 15% maximum baseline drift and 20% spike tolerance. Before collecting data, the cuvette was incubated in the

instrument for 5 min to allow the sample temperature to stabilize. The intensity of the size distribution was normalized to the peak value using OmniSIZE version 3.0 software, calculating the mean and standard deviation from the multiple scans (Viscotek).

Endotoxin Depletion and Quantification

Endotoxin was removed from all vaccine components using Triton X-114 phase separation (*60*, *61*). 1% (v/v) Triton X-114 was added to the protein on ice and incubated for 5 min. The solution was incubated at 37 °C for 5 min and centrifuged for 1 min at 16,000 g at 37 °C. The top phase was transferred to a fresh tube. This procedure was repeated for a total of three times. A final repetition without the addition of Triton X-114 was performed, to account for residual Triton X-114. A Pierce Chromogenic Endotoxin Quant Kit (Thermo Fisher) was used according to manufacturer instructions to quantify the final endotoxin concentration. All vaccine components were below the accepted endotoxin levels for vaccine products of 20 Endotoxin Units (EU) per mL (*62*).

Immunogen Preparation

The concentration of vaccine components was measured using BCA assay (Pierce). Where multiple antigens were coupled to the nanocage, the antigens were first mixed in equimolar amounts in TBS. Doses were normalized by the number of SpyTags, to facilitate an equimolar amount of SpyCatcher003-mi3 nanocages with similar occupancy in each condition. For high dose immunizations (Fig. S8-S10), SpyCatcher003-mi3 at 8 µM was incubated with 8 µM SpyTagged antigen for 48 h at 4 °C in TBS pH 8.0. For other immunizations, SpyCatcher003-mi3 at 0.8 µM was incubated with 0.8 µM total SpyTagged antigen for 48 h at 4 °C in TBS, pH 8.0. Uncoupled RBD and Uncoupled Quartet were incubated at 0.8 µM for 48 h at 4 °C in TBS pH 8.0, without the addition of SpyCatcher003-mi3. Prior to immunization, samples were analyzed by SDS-PAGE/Coomassie and DLS. For Fig. 5, SARS2 Spike prime and boost doses were performed with 10 µg SARS2 Wuhan Spike (HexaPro) protein in TBS pH 8.0 at 4 °C.

Mouse Immunization and Blood Sampling

Animal experiments were performed according to the UK Animals (Scientific Procedures) Act 1986, under Project License (PBA43A2E4 and PP9362617) and approved by the University of Oxford Animal Welfare and Ethical Review Body. Mice 6 weeks old (at the time of the first immunization) were obtained from Envigo. For high dose immunizations (Fig. S8-S10), we used BALB/c female mice and for all other immunizations we used C57BL/6 female mice. Mice were housed in accordance with the UK Home Office ethical and welfare guidelines and fed on standard chow and water *ad libitum*. Prior to immunization, immunogens were mixed 1:1 with VAC 20 adjuvant (SPI Pharma) (25 µL + 25 µL), except for the high dose immunizations (Fig. S8-S10) where immunogens were mixed 1:1 with AddaVax (Invivogen). This procedure gave final doses of 0.2 nmol total SpyTagged antigen for high dose immunizations and 0.02 nmol total SpyTagged antigen for normal dose immunization. For normal dose immunization, this relates to 0.6 µg Uncoupled RBD. Isoflurane (Abbott)-anesthetized mice were immunized on day 0 and day 14 intramuscularly in the gastrocnemius muscle with the specified antigen-adjuvant mix. Post-prime blood samples were obtained on day 13 via tail vein using Microvette (CB300, Sarstedt) capillary tubes. Post-boost samples were obtained on Day 32 to 41 (exact day for each set of immunizations is indicated in the figure) via cardiac puncture of humanely sacrificed mice. The collected whole blood in microtainer SST tubes (Becton Dickinson) was allowed to clot at 25 °C for 1-2 h, before spinning down at 10,000 g for 5 min at 25 °C. The sera were heat-inactivated at 56 °C for 30 min, before storing at −20 °C.

Enzyme-Linked Immunosorbent Assay (ELISA)

Nunc MaxiSorp plates (Thermo Fisher) were coated with 80 nM purified SpyTag-RBD, SpyTag-MBP or SpyCatcher003-mi3 in PBS (137 mM NaCl, 2.7 mM KCl, 10 mM Na_2HPO_4, 1.7 mM KH_2PO_4, pH 7.4) at 4 °C for 16 h. Where SARS2 was analyzed, this refers to the Wuhan variant, unless indicated. In Fig. S4B, the response to different SARS2 variants was measured by coating 1 µg/mL of the indicated HexaPro Spike protein in PBS and incubating at 4 °C for 16 h. Plates were washed three times with PBS supplemented with 1% (v/v) Tween 20 (PBST). Plates were blocked by 2 h incubation at 25 °C with 5% (w/v) skimmed milk in PBS. Plates were then washed three times with PBST. Sera were serially diluted into the blocking buffer using 8-point, 4-fold series starting at 1:100. Plates were incubated with sera for 1 h at 25 °C and then washed three times with PBST. Plates were incubated at 25 °C for 1 h with a 1:1,600 dilution of horseradish peroxidase-conjugated goat anti-mouse IgG antibody (Sigma-Aldrich A9044). Plates were washed three times with PBST. Plates were then incubated at 25 °C for 5 min with 1-Step™ Ultra TMB-ELISA Substrate Solution (Thermo Scientific) before the reaction was stopped with 1 M H_2SO_4. A_{405} measurements were taken with a FLUOstar Omega plate reader (BMG Labtech) using Omega MARS software (BMG Labtech). A sigmoidal dose response curve was fit to the absorbance data using the optimize.curve_fit() function from the Python SciPy library (*63*). The sigmoidal dose response function was:

$$y = \text{Bottom} + \frac{\text{Top} - \text{Bottom}}{1 + 10^{\log_{10}(\text{IC}_{50}) - x}}$$

The area under the fitted curve (AUC) was determined using the trapz function from the Python Numpy library (*64*). Area under the curve was used instead of endpoint titer to account better for data across the entire range of values (*65*). Results were plotted using GraphPad Prism (GraphPad Software version 9.4.1).

Microneutralization Assay

These assays were performed in the James & Lillian Martin Centre, University of Oxford, operating under license from the Health and Safety Authority, UK, on the basis of an agreed Code of Practice, Risk Assessments (under the Advisory Committee on Dangerous Pathogens) and standard operating procedures. The microneutralization assay determines the serum concentration that induces a 50% reduction in focus-forming units of SARS2 in Vero cells (American Type Culture Collection, CCL-81). A serial dilution of immunization sera [seven steps from 1/40 to 1/40,000 diluted into Dulbecco's Modified Eagle Medium (DMEM)] was pre-incubated for 30 min at 25 °C with a fixed dose of 100-200 focus-forming units (20 µL) of different authentic SARS-CoV-2 variants. This procedure was performed in triplicate for samples from high dose immunizations outlined in Fig. S8-S10 and in quadruplicate for all other samples. DMEM on its own was used for serum-free control wells, which were used to define 100% infectivity. The Victoria 01/2020 isolate (Pango B) was used for Wuhan neutralization (*66*). The Beta variant (Pango B.1.351) used for neutralizations is the HV001 isolate, sequenced and kindly supplied by CAPRISA, Durban, South Africa (*67*). The isolates for Delta (Pango B.1.617.2), Omicron BA.1 (Pango B.1.1.529.1), and Omicron BQ.1.1 (Pango B.1.1.529.5.3.1.1.1.1.1.1) were kindly supplied by Gavin Screaton (University of Oxford). This mixture was incubated with 100 µL of Vero cells (4.5×10^4) at 37 °C with 5% (v/v) CO_2. 2 h into this incubation, a 1.5% (w/v) carboxymethyl cellulose-containing overlay was applied in order to prevent satellite focus

formation. 18 h post-infection, the monolayers were fixed with 4% (w/v) paraformaldehyde in PBS and then permeabilized with 2% (v/v) Triton X-100. The cells were stained using the FB9B monoclonal antibody at 1 µg/mL (*68*). These samples were developed using an anti-human IgG (Fc-specific) peroxidase-conjugated antibody (1:5,000 dilution, cat. no. A0170-1ML, Sigma-Aldrich) and True Blue peroxidase substrate. The infectious foci were enumerated by Classic ELISpot Reader (AID GmbH). Data were analyzed using four-parameter logistic regression (Hill equation) using GraphPad Prism (GraphPad Software version 8.3). Statistical significance of differences between groups was determined using a one-way analysis of variance (ANOVA) test, followed by Tukey's multiple comparison post hoc test of ID_{50} values converted to log_{10} scale using GraphPad Prism (GraphPad Software version 9.4.1).

Pseudovirus Neutralization Assay

SARS2 BQ.1.1, SARS1, WIV1, SHC014, and BtKY72 K493Y/T498W pseudotyped viruses were prepared as described (*69*, *70*). The double mutation BtKY72 K493Y/T498W in the BtKY72 Spike protein has previously been shown to enable entry to human cells via ACE2 (*26*). This technique for producing pseudoviruses employs HIV-based lentiviral particles with genes encoding the appropriate Spike protein lacking the cytoplasmic tail. A three-fold serial dilution of sera was incubated with pseudotyped virus for 1 h at 37 ˚C. The mixture was incubated with $293T_{ACE2}$ target cells for 48 h at 37 ˚C (*6*). Cells were washed twice with PBS, before being lysed with Luciferase Cell Culture Lysis 5× reagent (Promega). NanoLuc Luciferase activity in the lysates was measured using the Nano-Glo Luciferase Assay System (Promega). The relative luminescence units (RLUs) were normalized to values derived from cells infected with pseudotyped virus in the absence of serum. Half-maximal inhibitory dilution (ID_{50}) was determined using 4-parameter nonlinear regression in AntibodyDatabase (*71*) and plotted using using GraphPad Prism (GraphPad Software version 9.4.1). Statistical significance of differences between groups was determined using an ANOVA test, followed by Tukey's multiple comparison post hoc test of ID_{50} values converted to log_{10} scale using GraphPad Prism (GraphPad Software version 9.4.1).

Bioinformatics

The phylogenetic tree of sarbecovirus RBD sequences was constructed using MEGA X v 11.0.13 software (*72*). Multiple sequence alignment and calculation of amino acid identity was performed using Clustal Omega v 1.2.4 (*73*). The structure of SARS2 RBD was based on PDB ID: 6ZER (*74*) and analyzed using PyMOL version 2.5.2.

Statistics and Reproducibility

No statistical method was used to predetermine sample size. Significance for ELISAs was calculated with an ANOVA test using Tukey's post hoc test in GraphPad Prism (GraphPad Software version 9.4.1). Comparisons for neutralizations were calculated with an ANOVA test, followed by Tukey's multiple comparison post hoc test of ID_{50} values converted to log_{10} scale using GraphPad Prism (GraphPad Software version 9.4.1). Stars were assigned according to: * $p < 0.05$, ** $p < 0.01$, *** $p < 0.001$. On graphs where some conditions are compared, where no test is marked then the difference was non-significant. The experiments were not randomized. The Investigators were not blinded to allocation during experiments and outcome assessment.

```
         320                 340                 360                 380                 400
Rs4081   RVSPTHEVVRFPNITNRCPFDKVFNASRFPNVYAWERTKISDCVADYTVLYNS-TSFSTFKCYGVSPSKLIDLCFTSVYADTFL
RmYN02   RILPSTEVVRFPNITNFCPFDKVFNATRFPNVYAWQRTKISDCIADYTVLYNS-TSFSTFKCYGVSPSKLIDLCFTSVYADTFL
Rf1      RVSPVTEVVRFPNITNLCPFDKVFNATRFPSVYAWERTKISDCVADYTVFYNS-TSFSTFNCYGVSPSKLIDLCFTSVYADTFL
BM-4831  RVTPTTEVVRFPNITQLCPFNEVFNITSFPSVYAWERMRITNCVADYSVLYNSSASFSTFQCYGVSPTKLNDLCFSSVYADYFV
BtKY72   RVSPSTEVVRFPNITNLCPFGQVFNASNFPSVYAWERLRISDCVADYAVLYNSSSSFSTFKCYGVSPTKLNDLCFSSVYADYFV
pang17   RVQPTISIVRFPNITNLCPFGEVFNASKFASVYAWNRKRISNCVADYSVLYNS-TSFSTFKCYGVSPTKLNDLCFTNVYADSFV
SARS2    RVQPTESIVRFPNITNLCPFGEVFNATRFASVYAWNRKRISNCVADYSVLYNS-ASFSTFKCYGVSPTKLNDLCFTNVYADSFV
RaTG13   RVQPTDSIVRFPNITNLCPFGEVFNATTFASVYAWNRKRISNCVADYSVLYNS-TSFSTFKCYGVSPTKLNDLCFTNVYADSFV
SHC014   RVAPSKEVVRFPNITNLCPFGEVFNATTFPSVYAWERKRISNCVADYSVLYNS-TSFSTFKCYGVSATKLNDLCFSNVYADSFV
SARS1    RVVPSGDVVRFPNITNLCPFGEVFNATKFPSVYAWERKKISNCVADYSVLYNS-TFFSTFKCYGVSATKLNDLCFSNVYADSFV
WIV1     RVAPSKEVVRFPNITNLCPFGEVFNATTFPSVYAWERKRISNCVADYSVLYNS-TSFSTFKCYGVSATKLNDLCFSNVYADSFV
         *: *  .::******: ***..*** : * .****:* :*::*:***:*:*** : ****:***** :** ****:.**** *:

                     420                 440                 460                 480
Rs4081   IRSSEVRQVAPGETGVIADYNYKLPDDFTGCVIAWNTAKQDQG-----QYYYRSSRKTKLKPFERDLTSDE-------------
RmYN02   IRFSEVRQIAPGETGVIADYNYKLPDDFTGCVLAWNTAQQDIG-----SYFYRSHRAVKLKPFERDLSSDE-------------
Rf1      IRFSEVRQVAPGQTGVIADYNYKLPDDFTGCVIAWNTAKQDVG-----SYFYRSHRSSKLKPFERDLSSEE-------------
BM-4831  VKGDDVRQIAPAQTGVIADYNYKLPDDFTGCVIAWNTNSLDS--SNE--FFYRRFRHGKIKPYGRDLSNVLFNPSGGTCSA-EG
BtKY72   VKGDDVRQIAPAQTGVIADYNYKLPDDFTGCVLAWNTNSVDSKSGNN--FYYRLFRHGKIKPYERDISNVLYNSAGGTCSSISQ
pang17   VKGDEVRQIAPGQTGVIADYNYKLPDDFTGCVIAWNSVKQDALTGGNYGYLYRLFRKSKLKPFERDISTEIYQAGSTPCNGQVG
SARS2    IRGDEVRQIAPGQTGKIADYNYKLPDDFTGCVIAWNSNNLDSKVGGNYNYLYRLFRKSNLKPFERDISTEIYQAGSTPCNGVEG
RaTG13   ITGDEVRQIAPGQTGKIADYNYKLPDDFTGCVIAWNSKHIDAKEGGNFNYLYRLFRKANLKPFERDISTEIYQAGSKPCNGQTG
SHC014   VKGDDVRQIAPGQTGVIADYNYKLPDDFLGCVLAWNTNSKDSSTSGNYNYLYRWVRRSKLNPYERDLSNDIYSPGGQSCSA-VG
SARS1    VKGDDVRQIAPGQTGVIADYNYKLPDDFMGCVLAWNTRNIDATSTGNYNYKYRYLRHGKLRPFERDISNVPFSPDGKPCTP-PA
WIV1     VKGDDVRQIAPGQTGVIADYNYKLPDDFTGCVLAWNTRNIDATQTGNYNYKYRSLRHGKLRPFERDISNVPFSPDGKPCTP-PA
         :  .:***:**.:** **********:* ***:***:   *        : **  *  ::.*: **::.

                  500                 520                 540
Rs4081    -NGVRTLSTYDFYPNVPIEYQATRVVVLSFELLNAPATVCGPKLSTALVKNQCVNF
RmYN02    -NGVRTLSTYDFNPNVPLDYQATRVVVLSFELLNAPATVCGPKLSTQLVKNRCVNF
Rf1       -NGVRTLSTYDFNQNVPLEYQATRVVVLSFELLNAPATVCGPKLSTSLVKNQCVNF
BM-4831   LNCYKPLASYGFTQSSGIGFQPYRVVVLSFELLNAPATVCGPKQSTELVKNKCVNF
BtKY72    LGCYEPLKSYGFTPTVGVGYQPYRVVVLSFELLNAPATVCGPKKSTELVKNKCVNF
pang17    LNCYYPLERYGFHPTTGVNYQPFRVVVLSFELLNGPATVCGPKLSTTLVKDKCVNF
SARS2     FNCYFPLQSYGFQPTNGVGYQPYRVVVLSFELLHAPATVCGPKKSTNLVKNKCVNF
RaTG13    LNCYYPLYRYGFYPTDGVGHQPYRVVVLSFELLNAPATVCGPKKSTNLVKNKCVNF
SHC014    PNCYNPLRPYGFFTTAGVGHQPYRVVVLSFELLNAPATVCGPKLSTDLIKNQCVNF
SARS1     LNCYWPLNDYGFYTTTGIGYQPYRVVVLSFELLNAPATVCGPKLSTDLIKNQCVNF
WIV1      FNCYWPLNDYGFYITNGIGYQPYRVVVLSFELLNAPATVCGPKLSTDLIKNQCVNF
           .    *  *.*  .  : .*  **********:.******** ** *:*::****
```

* = fully conserved
: = strongly similar
. = weakly similar

Supplementary Fig. 1. Sarbecovirus RBD sequence alignment. Amino acid sequence alignment of sarbecovirus RBDs used in this study, numbered according to Spike protein of SARS2 Wuhan variant.

A Sarbecovirus RBD Protein Identity

Clade		Rs4081	RmYN02	Rf1	BM-4831	BtKY72	pang17	SARS2	RaTG13	SHC014	SARS1	WIV1
2	Rs4081	100	88	89	67	70	71	69	69	68	68	70
	RmYN02		100	90	67	70	69	69	68	69	69	70
	Rf1			100	70	70	71	71	70	70	70	71
3	BM-4831				100	83	70	72	71	77	74	75
	BtKY72					100	73	74	73	77	75	76
1b	pang17						100	87	88	77	75	75
	SARS2							100	90	76	73	76
	RaTG13								100	76	75	77
1a	SHC014									100	82	84
	SARS1										100	95
	WIV1											100

RBD Amino Acid Identity: 100%, 90%, 80%, 70%, 60%

B Map of Residue Conservation

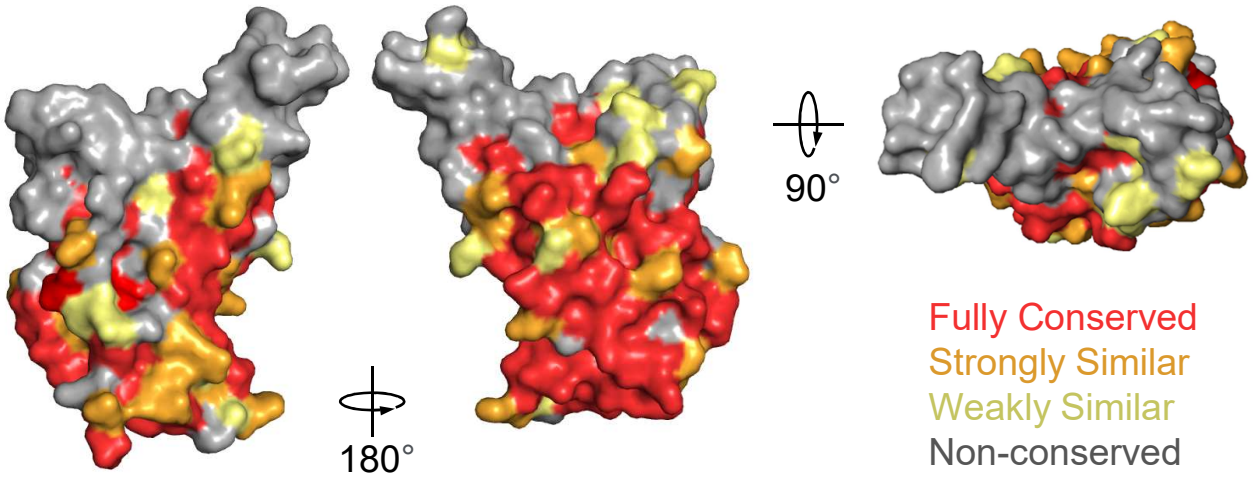

Supplementary Fig. 2. RBD residue conservation. (**A**) Heat map of percent amino acid identity between sarbecovirus RBDs used in this study. SARS2 refers to the Wuhan variant. (**B**) Conservation of residues between sarbecoviruses used in the study, as mapped onto the SARS2 RBD crystal structure (PDB ID: 6ZER). Multiple orientations of the same RBD are shown, represented as the van der Waals surface.

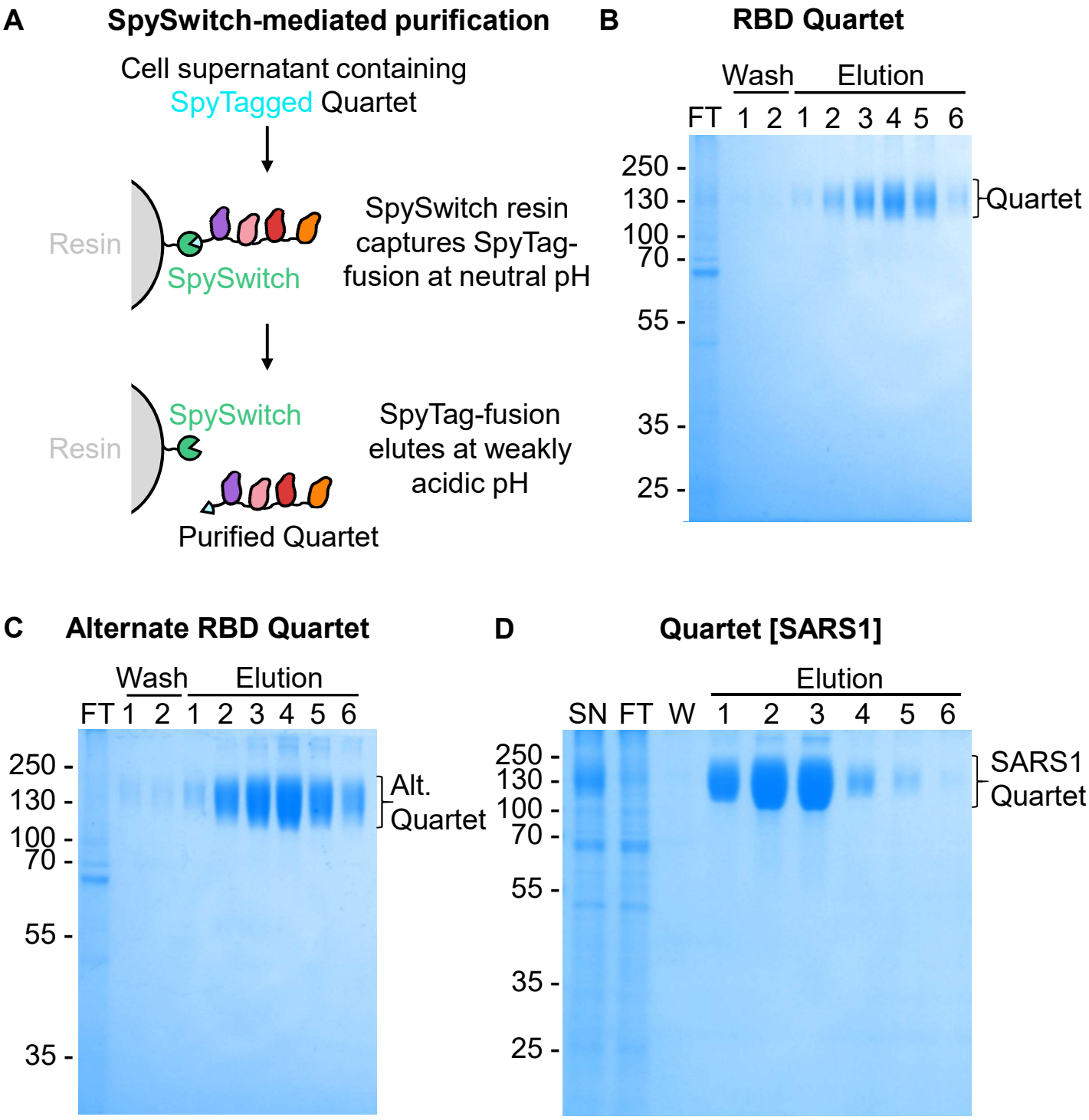

Supplementary Fig. 3. SpySwitch purification of RBD quartets. (**A**) Schematic of SpySwitch affinity purification. SpyTag genetically fused to the Quartet has a non-covalent interaction with SpySwitch at a neutral pH, before eluting at a weakly acidic pH through charge-charge repulsion. This system was used to purify (**B**) RBD Quartet, (**C**) Alternate RBD Quartet, and (**D**) RBD Quartet with SARS1 in place of SARS2. The supernatant (SN), flowthrough (FT), wash (W), and elution fractions were analyzed by SDS-PAGE with Coomassie staining.

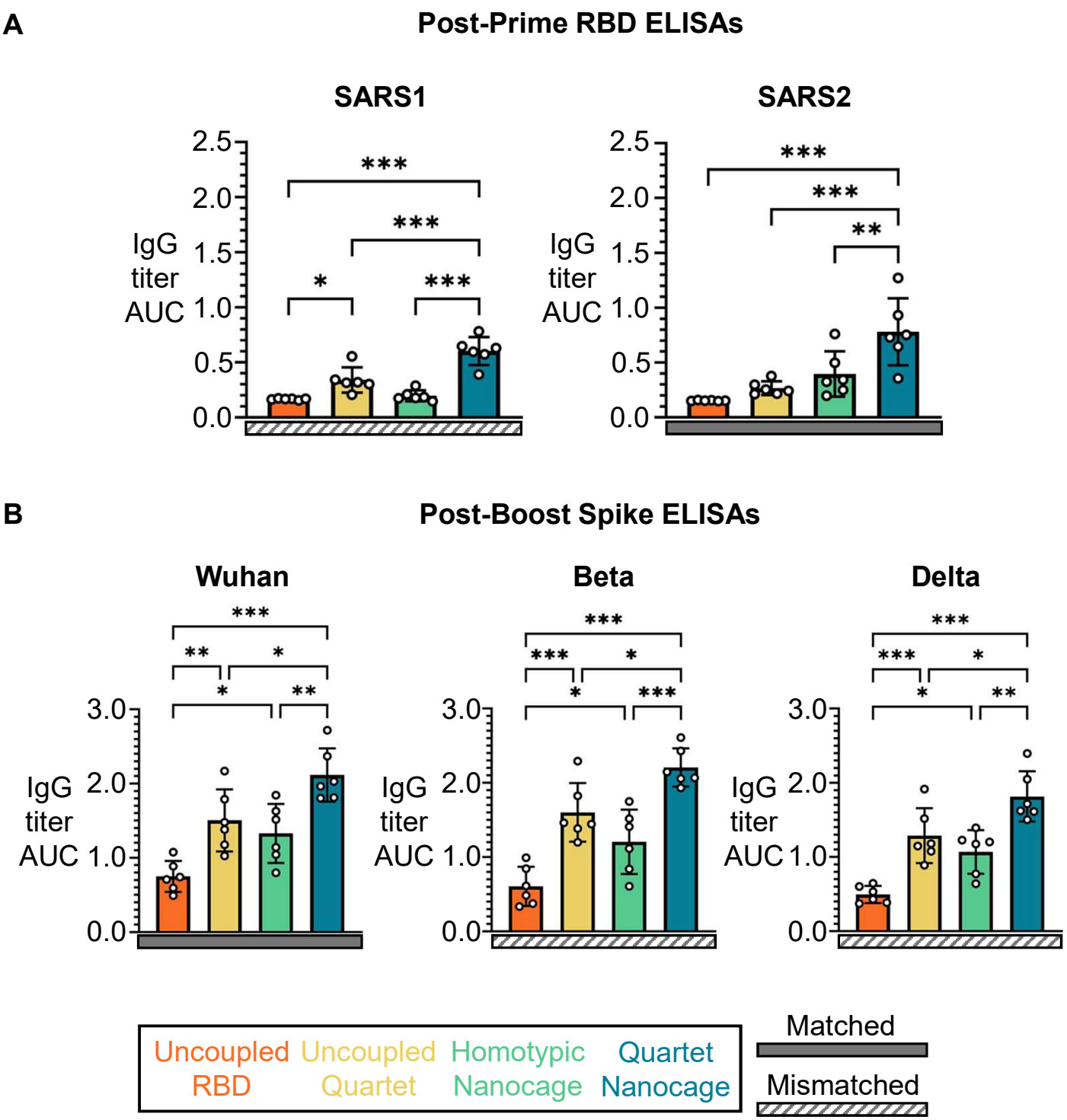

Supplementary Fig. 4. Further Breadth of Immune Response from Immunization with Quartet Nanocages. Binding data for serum IgG antibodies presented as area under the curve of a serial sera dilution. Sera samples are from mice immunized with uncoupled SARS2 RBD (orange), Uncoupled Quartet (yellow), SARS2 RBD coupled to SpyCatcher003-mi3 (Homotypic Nanocage, green), and Quartet Nanocage (blue) as outlined in Fig. 2. Solid gray rectangles under samples indicate the ELISA is against a component of that vaccine (matched), while striped rectangles indicate the ELISA is against an antigen absent in that vaccine (mismatched). Each dot represents sera from one animal. The mean is denoted by a bar, shown ± 1 s.d., n = 6. * $p < 0.05$, ** $p < 0.01$, *** $p < 0.001$; other comparisons were non-significant. Graphs demonstrate the binding of (**A**) post-prime sera to RBDs and (**B**) post-boost sera to SARS-CoV-2 variant Spike proteins.

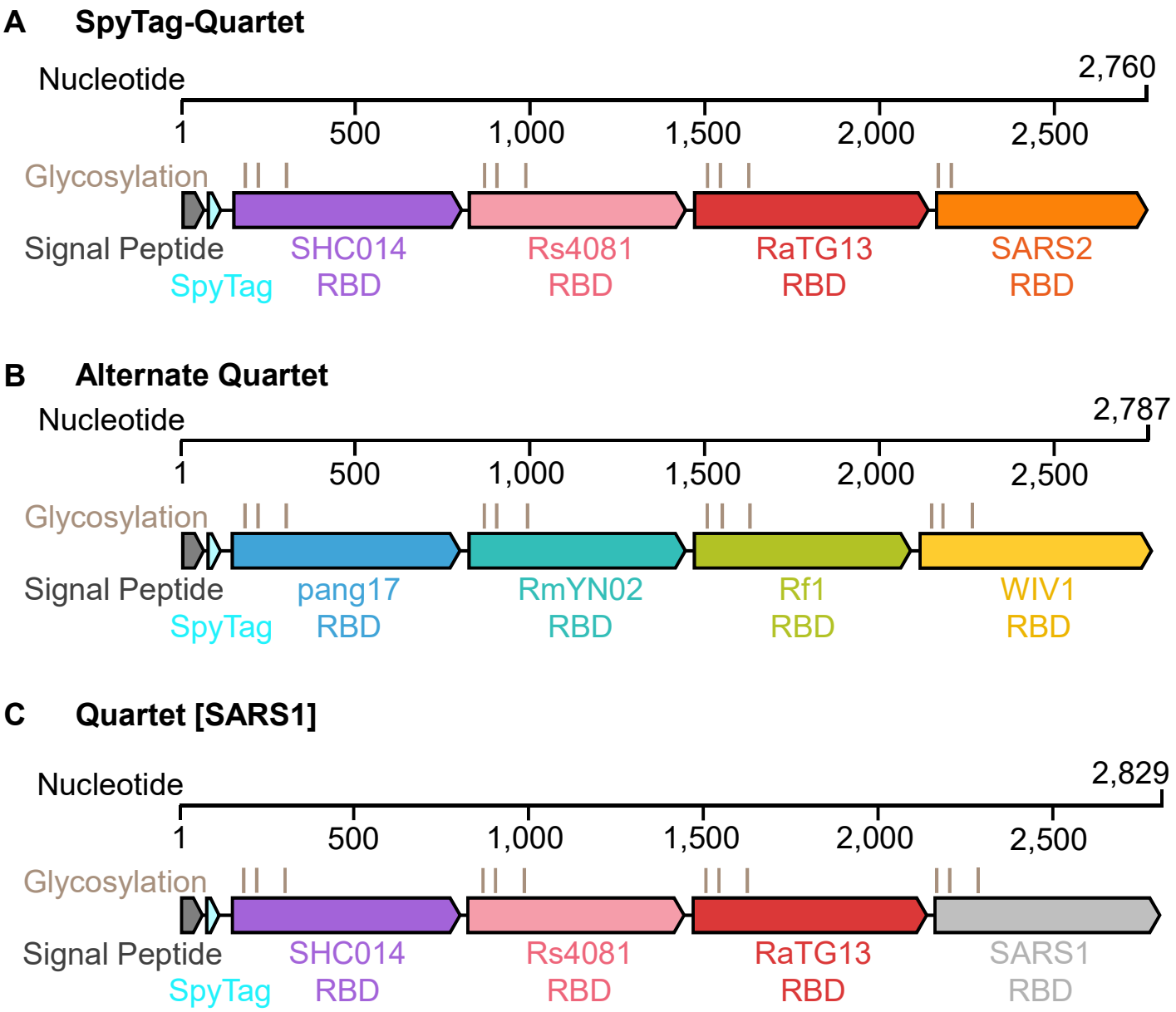

Supplementary Fig. 5. Schematic of Different Quartets. Genetic organization of (**A**) SpyTag-Quartet, (**B**) Alternate RBD Quartet, and (**C**) Quartet [SARS1]. These schematics indicate the virus origin of each RBD, predicted N-linked glycosylation sites, tag location, and nucleotide number for each construct.

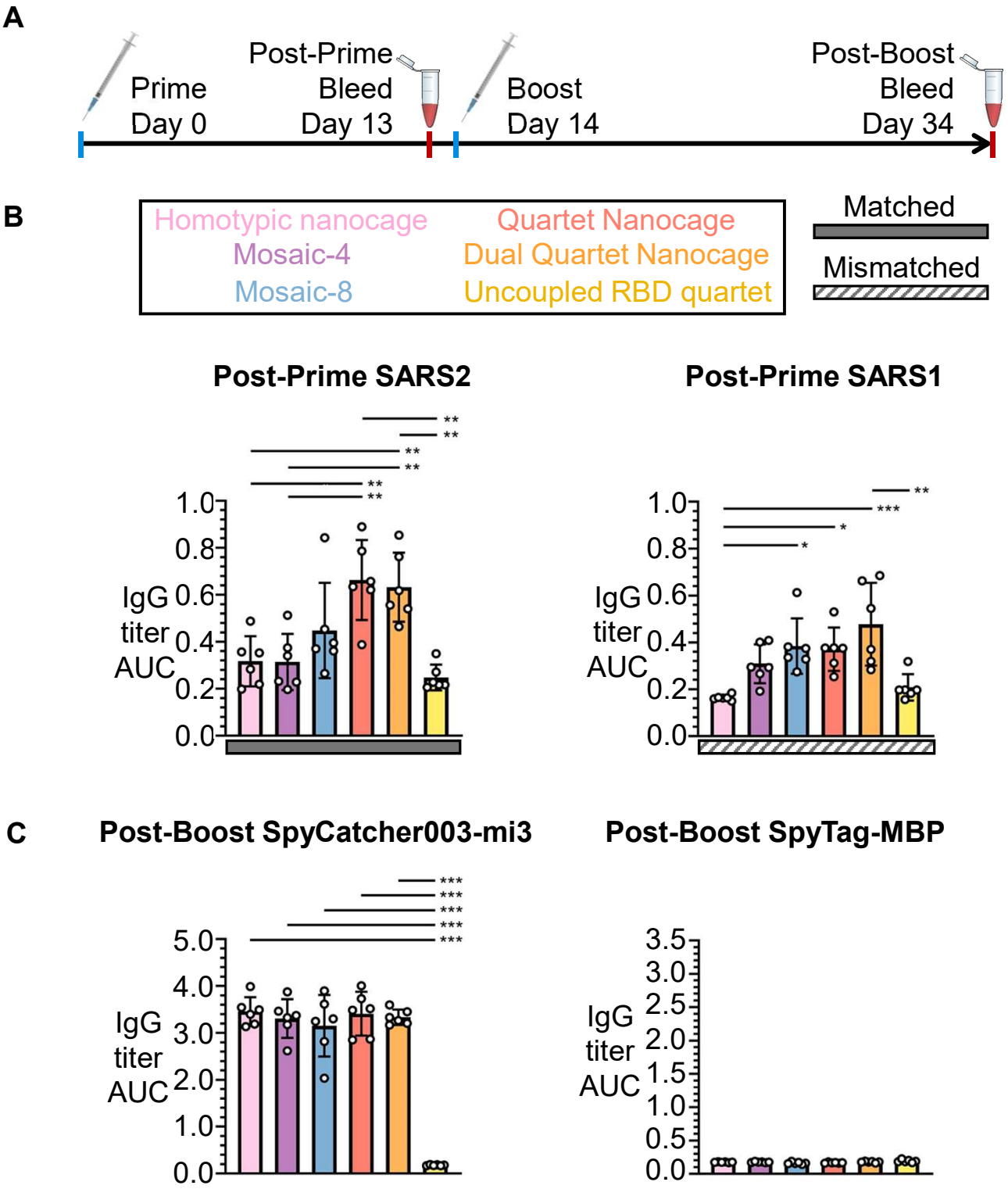

Supplementary Fig. 6. Breadth of antibody induction by Quartet and Mosaic Immunogens. (**A**) Summary of timeline for this set of immunizations with 0.02 nmol antigen per dose. **(B-C)** ELISA for serum IgG from mice immunized with the indicated immunogen. Each dot represents serum from one animal. The mean is denoted by a bar, with error bars ± 1 s.d., n = 6. * $p < 0.05$, ** $p < 0.01$, *** $p < 0.001$; other comparisons were non-significant. (**B**) Post-prime response to SARS2 or SARS1. (**C**) Post-boost response to SpyCatcher003-mi3 or SpyTag-MBP.

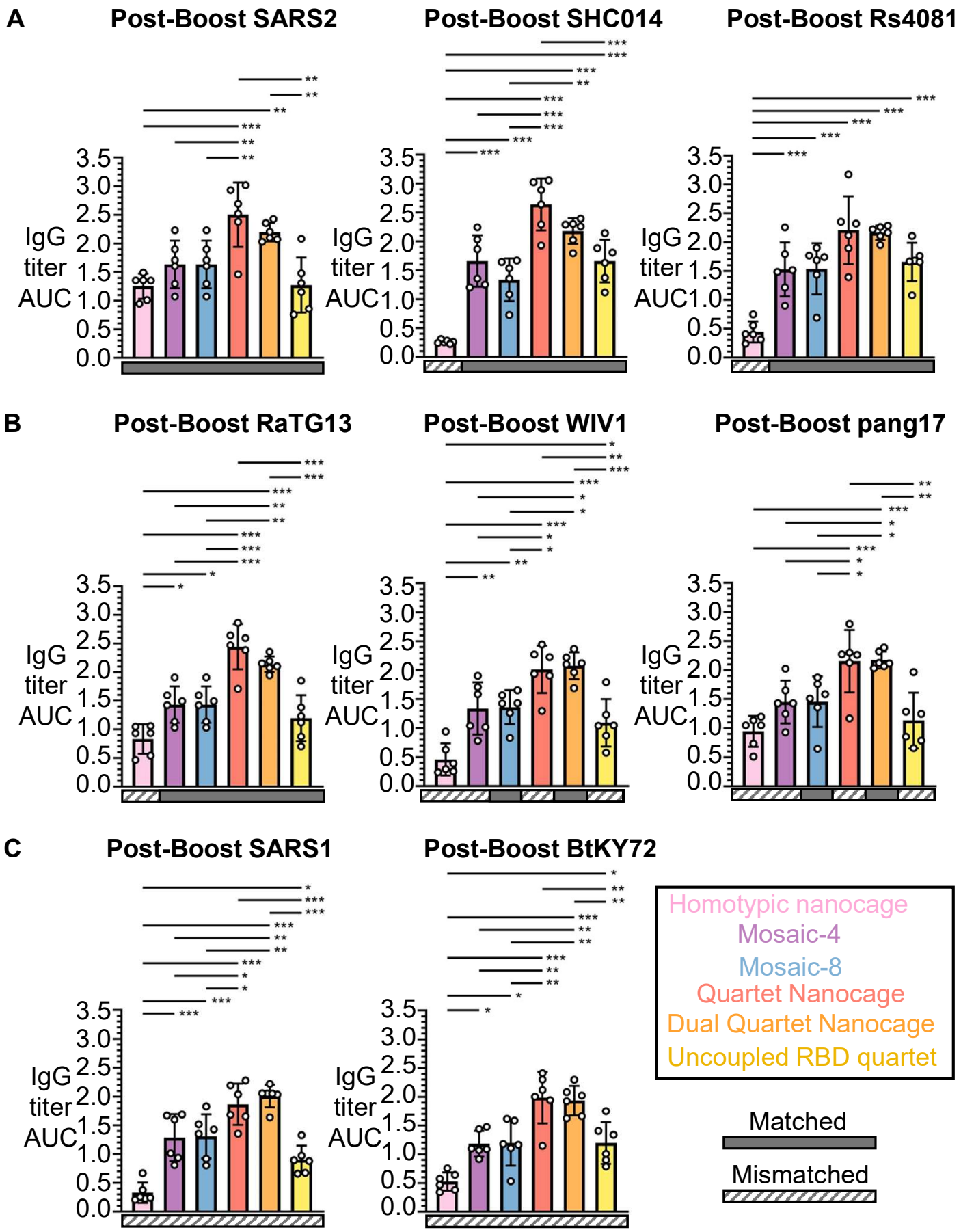

Supplementary Fig. 7. Further breadth of antibody induction by Quartet and Mosaic immunogens. ELISA for serum IgG from mice immunized with the indicated immunogen with 0.02 nmol antigen per dose. Each dot represents serum from one animal. The mean is denoted by a bar, with error bars ± 1 s.d., n = 6. * $p < 0.05$, ** $p < 0.01$, *** $p < 0.001$; other comparisons were non-significant. (**A**) Post-boost response to SARS2, SHC014 and Rs4081. (**B**) Post-boost response to RaTG13, WIV1 and pang17. (**C**) Post-boost response to SARS1 and BtKY72.

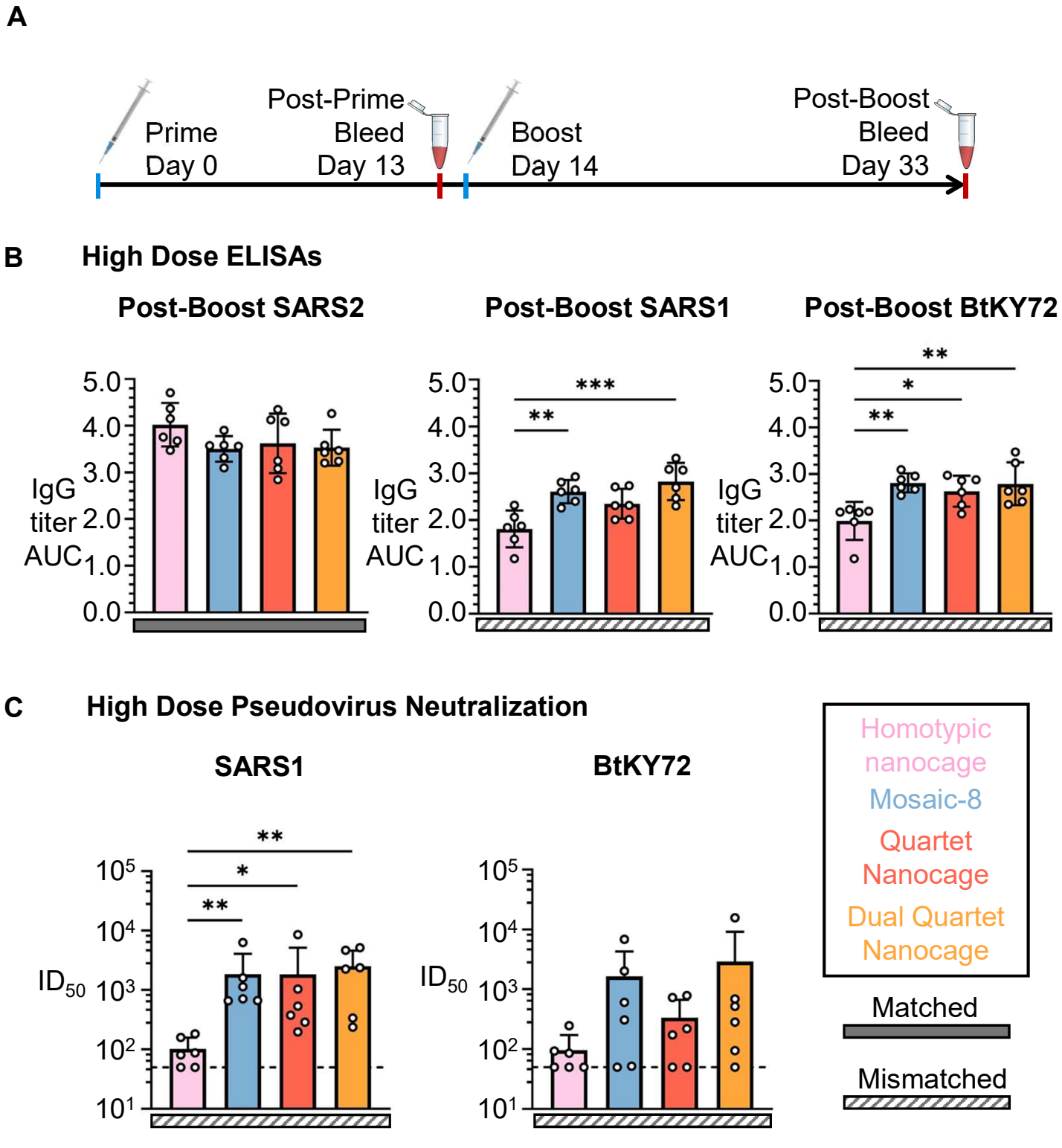

Supplementary Fig. 8. Immune response raised by higher dose of Quartet and Mosaic immunogens. This figure assesses antisera raised by immunizations with 0.2 nmol antigen. (**A**) Timeline for this set of immunizations. **(B)** ELISA for post-boost sera assessing IgG binding to SARS2, SARS1 and BtKY72 RBD is shown as the area under the curve (AUC) of a serial dilution. Each dot represents serum from one animal. The mean AUC is denoted by a bar, with error bars ± 1 s.d., n = 6. (**C**) Neutralization of SARS1 and BtKY72 (K493Y/T498W) pseudovirus by boosted mouse sera. Solid gray rectangles under samples indicate the ELISA is against a component of that vaccine (matched). Striped rectangles indicate the ELISA is against an antigen absent in that vaccine (mismatched). Dashed horizontal lines represent the limit of detection. The mean ID_{50} is denoted by a bar, with error bars + 1 s.d., n = 6. * $p < 0.05$, ** $p < 0.01$, *** $p < 0.001$; other comparisons were non-significant.

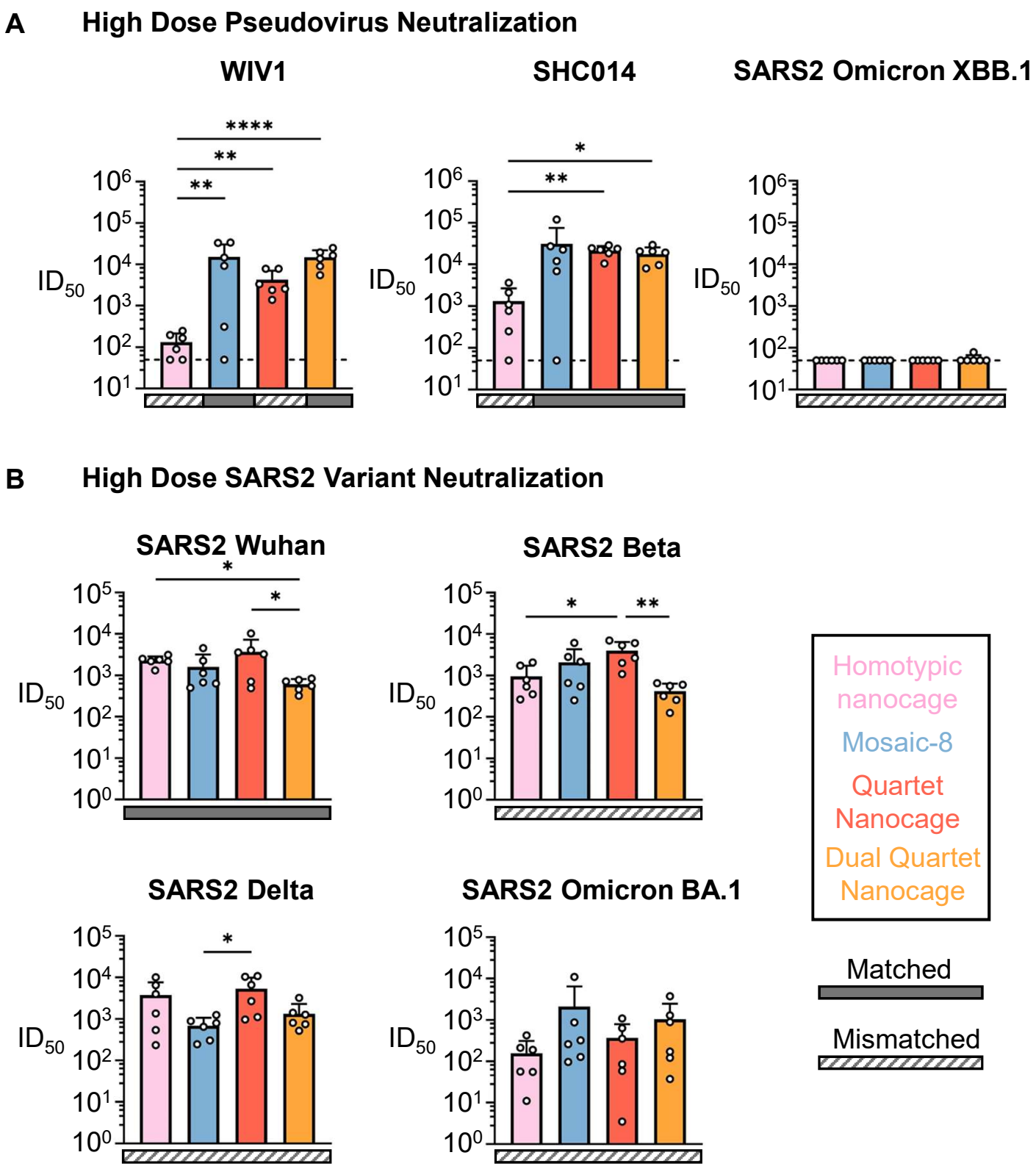

Supplementary Fig. 9. Pseudovirus neutralization by higher dose of Quartet and Mosaic immunogens. These figures assess antisera raised by immunizations with 0.2 nmol antigen, a 10x molar increase to antigen dose relative to prior immunizations. Solid gray rectangles under samples indicate the ELISA is against a component of that vaccine (matched). Striped rectangles indicate the ELISA is against an antigen absent in that vaccine (mismatched). Dashed horizontal lines represent the limit of detection. In all cases the mean ID_{50} is denoted by a bar, with error bars + 1 s.d., n = 6. * $p < 0.05$, ** $p < 0.01$, *** $p < 0.001$; other comparisons were non-significant. (**A**) Neutralization of WIV1, SHC014 and SARS2 Omicron XBB.1 pseudoviruses. **(B)** Neutralization of the Wuhan, Beta, Delta and Omicron BA.1 SARS2 variant viruses.

High Dose Virus Neutralization Curves

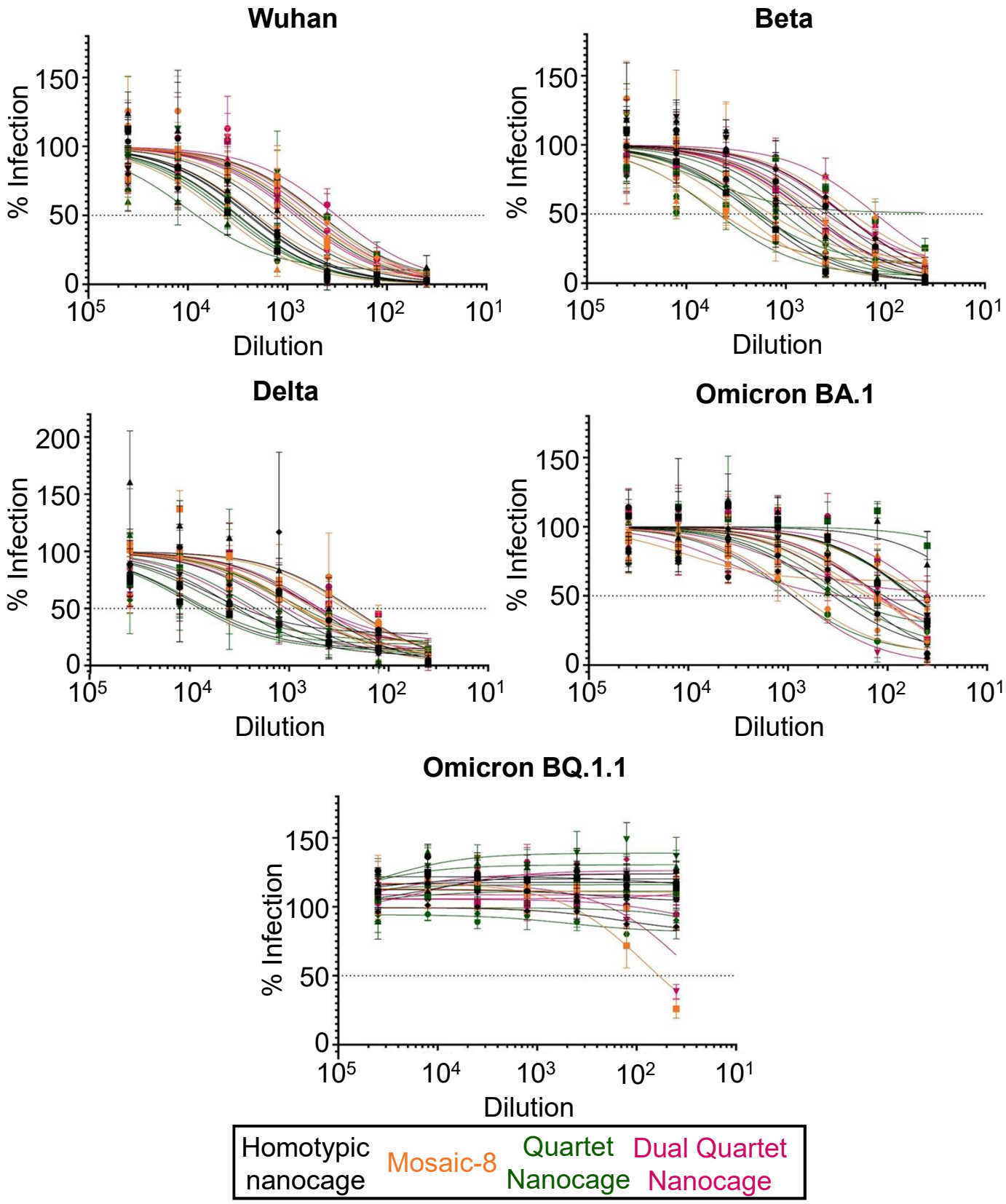

Supplementary Fig. 10. Authentic virus dose response curves. Neutralization of the Wuhan, Beta, Delta, Omicron BA.1, and Omicron BQ.1.1 SARS2 variants by antisera raised through immunizations with 0.2 nmol antigen. The percent of infection relative to a no-sera control (% Infection) was plotted relative to the dilution of sera. Each point is the mean of four replicates, with error bars ± 1 s.d., n = 6. These curves were used to determine the ID_{50} values plotted in Supplementary Fig. 9B. ID_{50} values could not be calculated for Omicron BQ.1.1.

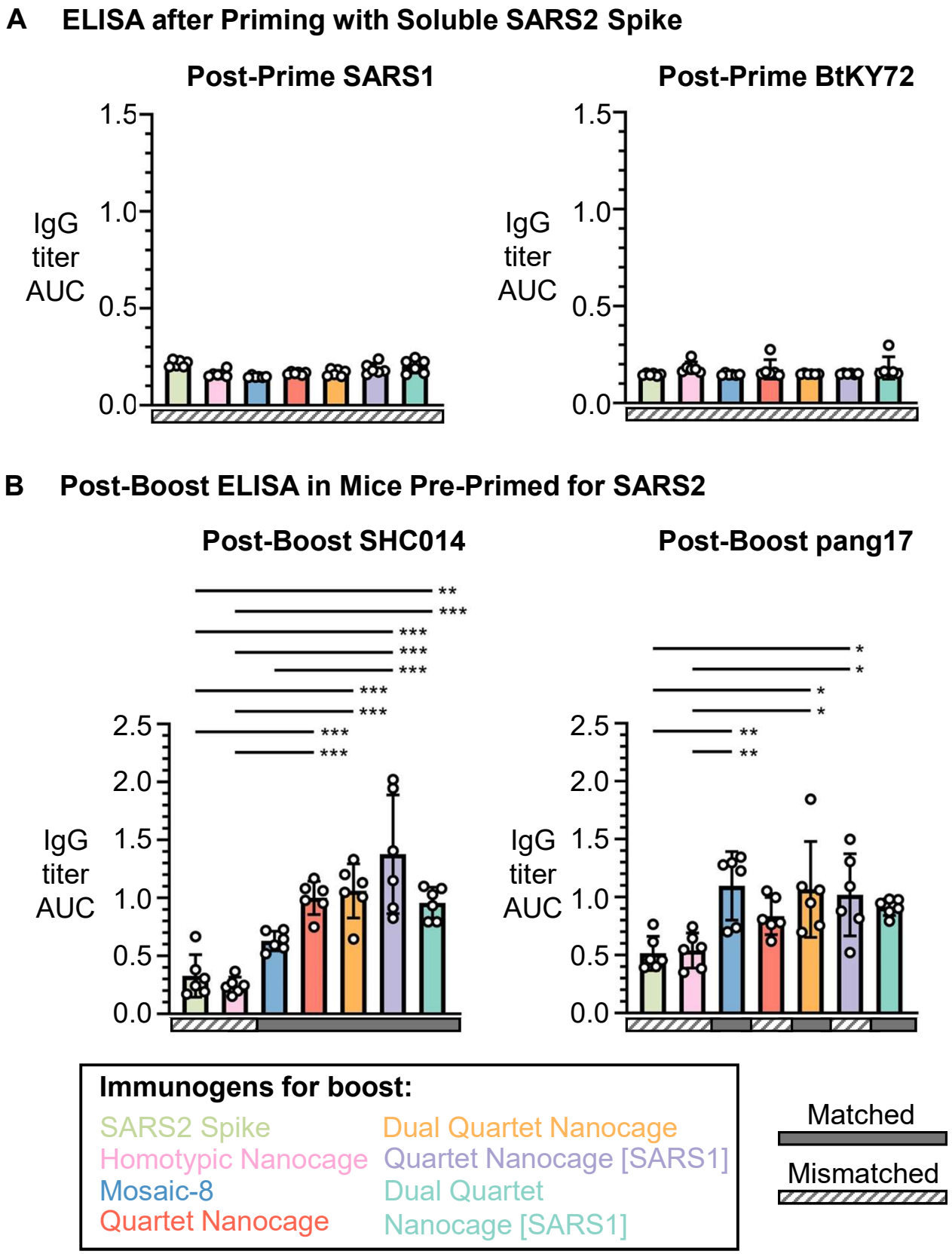

Supplementary Fig. 11. Further demonstration that Quartet immunization induces broad antibodies even after SARS2 Spike priming. (**A**) ELISA for serum IgG from mice immunized with a single dose of SARS2 Wuhan Spike protein, grouped by the second dose of 0.02 nmol antigen they will receive. (**B**) ELISA for serum IgG, after mice immunized with a single dose of SARS2 Wuhan Spike protein were boosted with a variety of different antigens at 0.02 nmol per dose. Each dot represents serum from one animal. The mean is denoted by a bar, with error bars ± 1 s.d., n = 6. * $p < 0.05$, ** $p < 0.01$, *** $p < 0.001$; other comparisons were non-significant.